A COMPARATIVE STUDY OF STEADY-STATE EFFECTIVE PERMEABILITY CALCULATION METHODS IN NATURALLY FRACTURED RESERVOIR

A Thesis in partial fulfillment of the requirements for the degree
Master of Science in Petroleum Engineering

Master Thesis submitted to
Department of Mineral Resources and Petroleum Engineering
Chair of Reservoir Engineering
University of Leoben

Under supervision of
Univ.-Prof. Dipl. Geol. PhD. Stephan K. Matthäi
Dipl.-Ing. Lang, Philipp

Jiyu Wang, B.Sc.

October 2012

ABSTRACT

   This thesis presents ways to estimate the effective permeability of naturally fractured reservoir under Discrete Fracture and Matrix Model (DFM). A Simple homogenous, steady state model, that contains an injection well and a production well at a certain distance, is firstly introduced. The pressure of the injection well can be estimated by analytical solution or numerical solution. The analytical solution is based on Darcy's law combined with the principle of superposition and used to interpret pressure and rate response by applying reservoir homogenization. The numerical solution is based on the Finite Element Method (FEM), as implemented in CSMP++. FEM model is used to get pressure and rate response in the case where analytical model does not exist, but this response is interpreted in terms of analytical models to estimate equivalent permeability. The pressure response estimated from analytical solution and numerical solution is compared. After comparison, models with varied fracture properties (geometry, intensity, size) are run with CSMP++. For radial flow, spherical flow and linear flow, the effective permeability is estimated by converted Darcy's law equation, once the pressure of injection well solved by CSMP++. But this can only be done for the homogeneous case, because the only case for which an analytical solution has been found previously. The injector-producer pair of wells in all models is with arbitrary completion length, because the height of the formation is not known. This pairs of wells have been operated long enough at a constant rate, so that a steady-state flow exists.

   The tasks accomplished by this thesis are (a). Use of homogeneous model verifies numerical method with analytical method. The difference between them is no more than 5% for models without fractures. Only with the numerical method, we can solve The permeability in complex DFM models, so that look for the equivalent k of DFM. (b). Through FEM analysis, the influence of fracture properties on the effective permeability is measured. Fracture size distribution and fracture orientation also play an important role for effective permeability. (c). The effective permeability estimated in linear flow is used as benchmark. Both radial and spherical flow interpretations result in an overestimated effective permeability. (d). The appropriate value of maximum element size is balancing simulation time and accuracy is analyzed as well.

(e). Circumscribed triangle well in numerical models represents circular well in analytical methods.

From the DFM simulations, it is found the parameters of power law distribution contribute to mean fracture size distribution.

ZUSAMMENFASSUNG

Diese Arbeit präsentiert Möglichkeiten, um die effektive Permeabilität von natürlich geklüfteten Reservoir unter Discrete Fracture und Matrix Model (DFM) zu schätzen. Ein einfaches homogenene, eingeschwungen Modell, das eine Injektionsbohrung und eine Produktionsbohrung in einem bestimmten Abstand enthält, wird zunächst intrroduced. Der Druck der Injektionsbohrung kann durch analytische Lösung oder numerische Lösung abgeschätzt werden. Die analytische Lösung basiert auf Darcy's law mit dem Prinzip der Superposition kombiniert und verwendet werden, um Druck und Fließrate durch Anlegen Reservoir Homogenisierung interpretieren basiert. Die numerische Lösung basiert auf der Finite-Elemente-Methode (FEM), wie in CSMP++ implementiert. FEM-Modell wird verwendet, um Druck und Fließrate in dem Fall, analytisches Modell nicht existiert bekommen, aber diese Respons ist in Bezug auf analytische Modelle zu interpretieren, um äquivalente Permeabilität zu schätzen. Der Druck Respons von analytischen Lösung und numercial Lösung geschätzt wird verglichen. Nach Vergleich werden Modelle mit unterschiedlichen Brucheigenschaften (Geometrie, Intensität, Größe) mit CSMP++ laufen. Für strahlenförmig, sphärische und linearen Strömung, der äquivalente Permeabilität durch umgewandelten Darcy's law Gleichung geschätzt wird, sobald der Druck der Einspritzung gut durch CSMP++ gelöst. Dies kann aber nur für die homogene Fall durchgeführt werden, da der einzige Fall für die eine analytische Lösung wurde zuvor festgestellt worden. Der Injektor-Produzent Paar von Vertiefungen in allen Modellen mit beliebigen Fertigstellung Länge, da die Höhe der Formation nicht bekannt ist. Diese Paare von Vertiefungen wurden lange genug mit einer konstanten Geschwindigkeit betrieben, so dass eine eingeschwungen Strömung herrscht.

Die Aufgaben dieser Arbeit erreicht sind (a). Verwendung homogener Modell numerische Verfahren mit analytischen Verfahren zu überprüfen. Der Unterschied zwischen ihnen nicht mehr als 5% für Modelle ohne Frakturen. Nur mit der numerischen Methode können wir die effektive Permeabilität in komplexen DFM Modellen zu lösen, so dass den Gegenwert k im DFM Modellen is gesucht. (b). Durch FEM-Analyse ist der Einfluß der Brucheigenschaften auf die effektive Permeabilität gemessen. Fraktur Größenverteilung und Spaltenorientierung spielen auch eine wichtige Rolle für die effektive Permeabilität. (c). Der effektive

Permeabilität im linearen Fluss geschätzt wird als Referenzwert verwendet. strahlenförmig als auch sphärische Strömung führen in einem überschätzt effektive Permeabilität. (d). Der passenden Wert der maximalen Elementgröße balanciert Simulationszeit und Genauigkeit sowie analysiert. (e). Umschriebene Dreieckig Bohrloch in numerischen Modellen stellt kreisförmigen Bohrloch in der analytischen Methoden dar.

Aus den DFM-Simulationen ist es die Parameter des Power-law Verteilung verursachen durchschnittliche Bruchgrößenverteilung.

AFFIDAVIT

I hereby declare that this master thesis has been written only by the undersigned and without any assistance from third parties.

Furthermore, I confirm that no sources have been used in the preparation of this thesis other than those indicated in the thesis itself.

_____   _____

Date   Signature

ACKNOWLEDGEMENTS

First and foremost, I would like to show my deepest gratitude to my supervisor, Prof. Stephan K. Matthäi, a respectable, responsible and resourceful scholar, who has provided me with valuable guidance in every stage of the writing of this thesis. Without his enlightening instruction, impressive kindness and patience, I could not have completed my thesis. His keen and vigorous academic observation enlightens me not only in this thesis but also in my future study.

I shall extend my thanks to Dipl.-Ing Lang Philipp for all his kindness and help. Philipp spares his precious time to help me to create the models, run the simulation and modify structure of my thesis. I would also like to thank Dipl.-Ing. Seidl Georg and Dipl.-Ing. Trojer Mathias. At the time when I encounter difficulties, they will always lend a helping hand.

Last but not least, I'd like to thank all my friends, my family for their encouragement and support.

Table of Contents

List of Tables

List of Figures

1. Introduction

About a third of the worldwide oil and gas reserves occur in naturally fracture reservoirs (Bourbiaux, 2010). These are predominantly in carbonate reservoirs in the Middle East and northern Africa. A naturally fractured reservoir is defined as a reservoir in which naturally occurring fractures either have or are predicted to have an effect on fluid flow either in the form of increased reservoir permeability or increased permeability anisotropy (Nelson, 2001). These fractures are discontinuities in the rock that can be produced by deformation. They exist on various length scales from microns to kilometers. They appear as tensile (e.g. joints) or shear (e.g. faults) acting as hydraulic conductors or barriers to flow (Masihi and King, 2006)

In naturally fractured reservoirs, the equivalent permeability refers to a block permeability that depends on block geometry and boundary conditions when numerical methods are used to estimate it (Durlofsky, 1991). Effective permeability refers the characterization of a physical property in heterogeneous porous media (Nkashima and Sato, 2000). It will not be influenced by flow conditions, as opposed to equivalent permeabilities. It is associated with the concept of the representative elementary volume (REV) that applies to a stationary heterogonous property field.

In reservoir management, the knowledge of the reservoir permeability is essential for oil and gas production and needed to optimize well completion and field development. The permeability of a formation is vital to determine whether a well should be developed. The permeability of reservoir rock may be measured through laboratory testing of core sample (Mattews and Russel, 1967), well-logging of the reservoir (Earlougher, 1977) or well testing (Ahmed, 1989).

The estimation of the equivalent permeability in naturally fractured reservoirs given a specific production set-up can be achieved either by numerical methods based on the Discrete Fracture Network Approach (Gilmour and Witherspoon, 1985) or analytical solutions (Oda, 1985). Flow-based (homogenization) methods calculate equivalent permeability tensors that depend on the geometry of blocks and on flow boundary conditions applying to blocks on a DFM (Discrete Fracture-Matrix Model) realization. Analytical methods are an efficient way to approximate effective permeability tensors using only the geometry of the fractures. Thus Oda's method is

geometry based accounting for fracture densities and properties attached to grid blocks for effective permeability upscaling.

1.1 Review

Warren and Root (1963) think that fractures and matrix could be treated as two separate continuums in the domain, if the matrix is relatively permeable and the fractures are well interconnected. Snow (1969) thinks if fractures are well interconnected, they can be assumed to be infinite and dominate permeability, so that the matrix can be ignored.

Oda (1985) presented the permeability tensor k_{ij} can be concisely expressed by a symmetric, second-rank tensor P_{ij}, which depends on the geometrical properties of related fractures (size, orientation, shape, aperture). He also introduced the Kronecker delta to normalize fracture orientation relative to grid block geometry.

Robinson (1985) presented that the fractures are represented on an unstructured grid to preserve their original geometry and the flow rate is computed for specific boundary conditions to obtain the total flow through the fractures, which is a flow based method. This method, compared to Oda method, is of higher computational expense (flow simulation essential) and the result depends on the type of boundary conditions.

Durlofsky (1991) presented a numerical procedure for computing the effective permeability of a region of periodically distributed heterogeneity. This method solves pressure equation over the periodical unit subject to periodic boundary conditions and then upscales the velocity field to yield effective permeability.

Lough (1996) et al. proposed a method to estimate the effective permeability of grid blocks used in continuum simulation of naturally fractured reservoirs. The boundary element method was employed to solve the boundary integral equations for the pressure under periodic boundary conditions. They applied the method to a fracture system generated using statistical data of fracture length, orientation and intensity form an actual reservoir.

Matthai et al. (2008) presented an approach to compute effective permeability of fracture matrix system. The method is based on a finite element-based discretization using DFM. Effective permeability is computed by the Complex Systems Modeling Platform (CSMP++), which is an object-oriented finite-element based library for multi-physics modeling developed at Imperial College and the ETH Zurich.

1.2 Claim

This MSc thesis continues to study of effective permeability of fractured rock following approach of Matthai (2008). The tasks accomplished by this thesis are (a) Using homogeneous model to verify numerical method with analytical method. The difference between them is no more than 5% for models without fractures. Only with the numerical method, we can solve the permeability in complex DFM models, so that look for the equivalent k of DFM. (b) Through FEM analysis, the influence of fracture properties on the effective permeability is measured. Fracture size distribution and fracture orientation also play an important for effective permeability. (c) The effective permeability estimated in linear flow is used as benchmark. Both radial and spherical flow interpretations result in an overestimated effective permeability. (d) The appropriate value of maximum element size is balancing simulation time and accuracy is analyzed as well.

A box of known and invariable volume is assumed. This box consists of a matrix with uniform permeability. For simulation, three cases are assumed: two full complete wells (200 m length), two partial complete wells (5 m length) and no well. This pairs of wells have been operated long enough at a constant rate, so that a steady-state flow exists. I assume that flow rate of one well (injection well), pressure of one well (production well) and permeability of matrix is known. Therefore, the bottom-hole pressure of the injection well can be solved analytically and numerically. They are be compared in varies case (full well, partial well and no wells). After verification of numerical solution, 8 DFM models with variable fracture properties are run by CSMP++. The pressure of injection well can be solved again with DFM models in individual case. The effective permeability in the inter-well region can be estimated

by converted Darcy's law equation, when the pressure of injection well solved by CSMP++.

1.3 Agenda

Chapter 2 describes the methods used in accomplishing estimation of the effective permeability in single phase, stead state flow models. Chapter 3 presents the results and comparison of the simulation results. Chapter 4 gives a conclusion and discussion of finding from this thesis.

2. Methodology

2.1 Permeability

The concept of permeability is important in determining the flow characteristics of hydrocarbons in reservoir. The unit of permeability is "Darcy". 1 Darcy describes the capability of fluid with one cP viscosity flowing with rate of 1 cm^3/s through sample, its length of 1 cm and cross section area of 1 cm^2, under 1 atm/cm pressure drop(see Figure 1). The SI unit of permeability is m^2. The unit of Darcy to m^2 relates as follows:

$$1\,\text{Darcy} = \frac{1cP \cdot 1cm^3 / s \cdot 1cm}{1cm^2 \cdot 1atm / cm} = 9.869233\text{e}^{-13} m^2 \approx 10^{-12} \text{ m}^2$$

For most reservoirs, permeabilities are less than 1 Darcy, therefore "mD" is more commonly used as the unit of permeability. A millidarcy (mD) is equal to 0.001 Darcy.
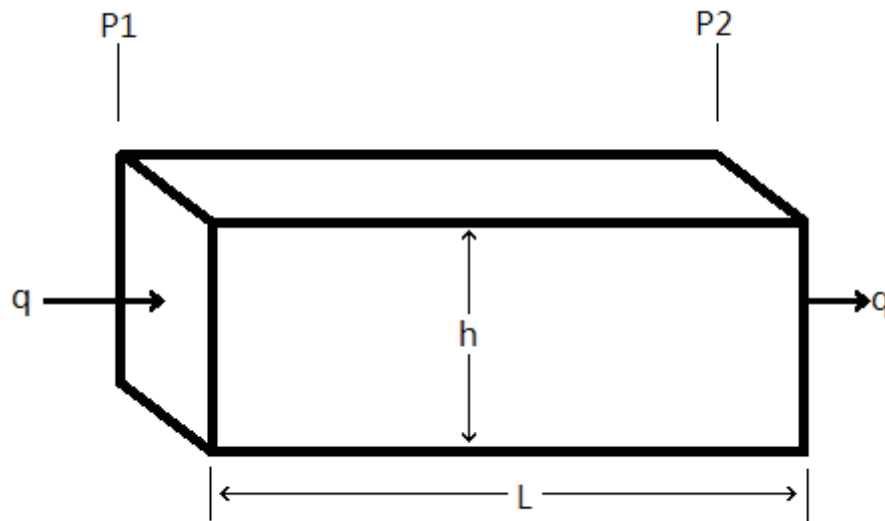
Figure 1: Linear, single phase, steady state flow through constant cross section box

Figure 1 illustrates Darcy's law applying for single phase fluid flow linear in homogenous region from left to right through a constant cross-sectional area, where both ends are open to flow. Fluid with constant flow rate q flows through the porous block with constant permeability k over a distance of L. The pressure at the ends of porous block drops from p_1 to p_2.

Darcy's law can be applied to estimate the permeability of porous media for laminar creeping, steady state, single phase flow (Tek, 1957). The differential form of Darcy's law is:

$$q = -\frac{AK}{\mu}\frac{dp}{dL}$$ 1

Where: q= flow rate under steady condition (m^3/s);

A= cross section area for porous medium (m^2);

μ= fluid viscosity (Pa˙s);

k= permeability of medium (m^2);

dp/dL= pressure gradient;

Equation 1 is a solution for linear flow. In linear flow, if the cross-section area is constant, the pressure drop required to induce a given flow rate is also constant. Equation 1 can be integrated using separation of variables to obtain the description of permeability as follow:

$$k = \frac{q\mu L}{A\Delta p}$$ 2

Where: Δp = pressure differential between both ends of rock sample

L = length of rock sample;

Following assumptions need be fulfilled for Darcy's law to be applicable:

- Saturated conditions (single phase) of sample

- Inert properties

- Laminar flow

- No volume change of fluid due to temperature change

2.2 Effective Permeability of Fracture Reservoir

The effective permeability is defined as arithmetic permeability in fine scale heterogeneities within the porous medium (Durlofsky, 1991). This is the basic

definition of effective permeability, but in our case, the effective permeability is mainly expressed as valid permeability in the model. Fracture and matrix permeability are combined in our model. Therefore, we consider it to be the ensemble permeabilities of matrix and fracture.
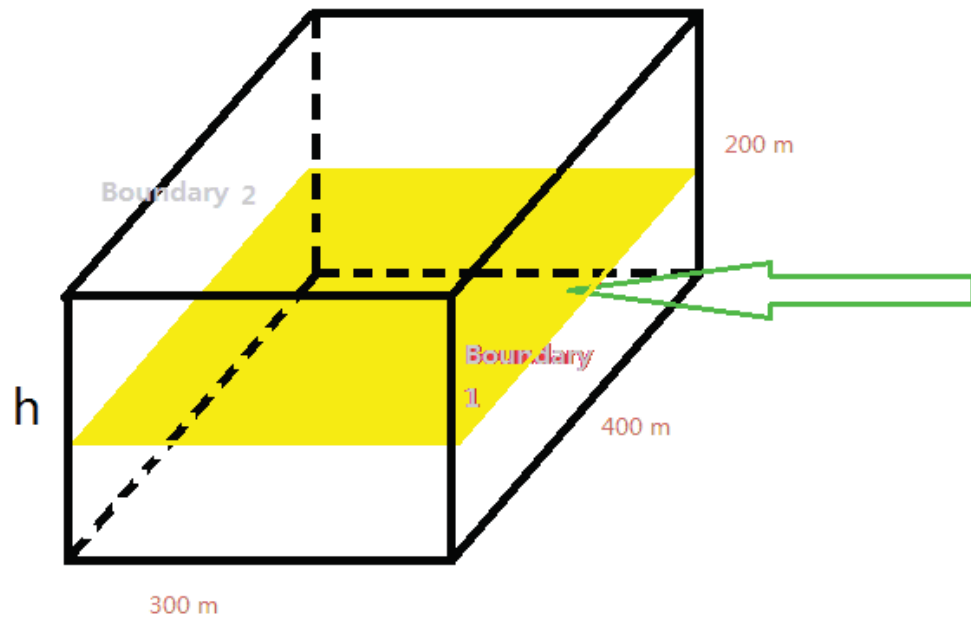
Figure 2: Single horizontal fracture (yellow area) in a box, fluid flow from bondary1 to boundary2

Figure 2 shows an illustrative model with a horizontal fracture and located in the middle of box. The matrix permeability of the box is k_m, the permeability of the fracture is k_f. The height of box is 200m and the aperture of fracture is 0.001 m. Arithmetic average method (Bear, 1972) can be utilized to calculate the effective permeability for the model (fracture and matrix):

$$k_{eff} = \frac{\sum_{1}^{n} k_i h_i}{\sum_{1}^{n} h_i} \quad \text{...} \quad 3$$

$$k_{eff} = \frac{0.001 \cdot k_2 + (200 - 0.001) \cdot k_1}{200} \quad \text{..................................} \quad 4$$

k_{eff} is the effective permeability for the model. k_1 is permeability of matrix, k_2 is permeability of fracture. Because the fracture in the model is single and simple, it was

estimated using arithmetic average, once the fluid flows from right to left. If fracture distribution and orientation are more complex, an analytical solution can not be avoided.

2.2.1 Calculation Methods

Two methods are commonly used to calculate effective permeability in the continuum block. They are the geometry-based (Oda, 1985) and the flow-based method (Robinson, 1984).

2.2.1.1 Geometry Based Method

Oda's method utilizes a geometric description of three dimensional discrete fracture networks in isotropic porous media. The orientation of fractures in each block of interest is expressed through normal vectors. It is assumed, that fractured rock masses behave similar to porous media and approximated by homogeneous and anisotropic properties within each control volume. The permeability tensors is then estimated and upscaled for each block of interest:

$$k_{ij} = \frac{1}{12}\left(F_{kk}\delta_{ij} - F_{ij}\right) \dotfill 5$$

Where k_{ij} = Permeability tensor

            F_{ij} = Fracture tensor

            δ_{ij} = Kroenecker delta

            F_{kk} = Total fractures

$$F_{ij} = \frac{1}{V}\sum_{k=1}^{N}\left(A_k T_k n_{ik} n_{jk}\right) \dotfill 6$$

Where F_{ij} = Fracture tensor

            V = Grid cell volume

            N = Total number of fractures in grid cell

            A_k = area of fracture k

            T_k = transmissivity of fracture k

$n_{ik}\ n_{jk}$ = the components of a unit normal to the fracture k

The permeability tensor k_{ij} is calculated directly by a fracture tensor F_{ij}, that depends on the geometrical properties of connected fractures. The advantage of Oda's method is that flow simulation is not required. However, it accounts only for well-connected fractures. Permeability tensor k_{ij} is sensitive to grid block sizes. Applying very fine discretization (mm scale grid cells), the Oda approximation produces the underlying discrete fracture hydro-structural model. But, At much coarser discretization (tens or hundreds of m grid-cells), Oda's approximation leads to less accurate results.

2.3.1.2 Flow Based Method

Compared to Oda's method that only considers interconnected fractures, effective permeability computed through flow based methods, can be of high accuracy even for poorly connected fractures. Steady state flow of incompressible fluid through the fracture is derived from law of mass conservation is given by:

$$\nabla \cdot u = 0 \dotfill 7$$

where u is flow velocity. In a simple model for flow through a fracture of parallel plate form, Darcy's law preserving the momentum of flow is extended to the cubic law:

$$v = \frac{a^2}{12l_f \mu} \frac{dp}{dx} \dotfill 8$$

Where a is fracture aperture, l_f is the fracture length, dp/dx is the pressure difference between the nodes. The fractures in flow based methods are represented to use unstructured grids to preserve their original geometry. The effective permeability from Darcy's law can be computed with Equation 8 for specific boundary conditions to obtain the total flow through the fractures. Flow based methods provide considerably more accuracy, even if the fractures are not interconnected. Compared to Oda method, flow simulation is required. Therefore the computational expenses are higher. The result is also dependent on the type of boundary conditions.

2.3.2 Representative Elementary Volume

The concept of the REV, which was introduced by Bear (1972), is essential to understand and evaluate petrophysical characteristics (e.g. porosity and permeability) of reservoir rocks. A fluid flow through a real porous medium is based on the assumption of a perfect porous equivalent continuum block. In fact, it is not feasible to measure petrophysical characteristics at any arbitrary point in the whole continuum block. General, we measure the value of properties from a small volume of samples to represent a large volume of samples. But if reservoir properties are established based on small volume samples, it is possible to randomly select a too low value. If the volume of the sample is not representative to the characterization of the whole samples of porosity, a bigger sample is necessary.
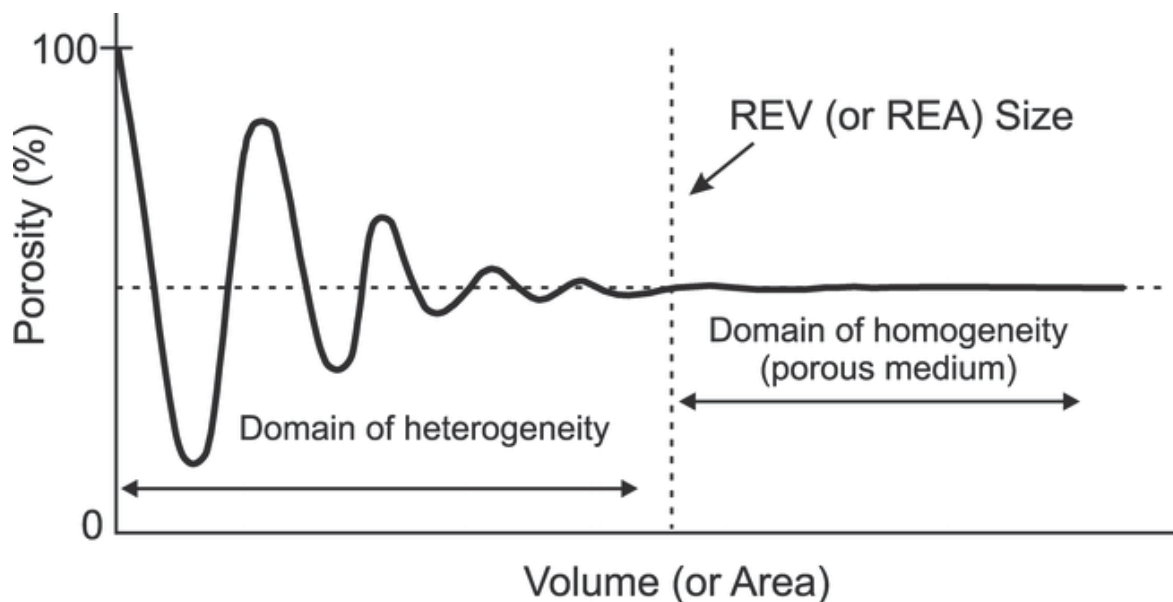
Figure 3: Representative Elementary Volume for porosity (Bear, 1972).

For the porous medium represented in Figure 3, the curve line of sample for which porosity does not characterize the entire volume of the rock masse, thus there are not representative. After the vertical dash line, the porosity becomes relatively constant, and can be considered representative. But for very large volumes, the representative feature is lost because of the inherent heterogeneity of domain.

To determine the scale of a REV for effective permeability, a detailed study of fracture network is necessary. REV is correlated with the fracture parameters such as total length, mean length and the mean orientation angle (Nordahl, 2008). A stochastic fracture distribution may be evaluated to assess the effective permeability

change as the area of the region is changed. The critical area for a representative value of effective permeability in REV increases in proportion to the mean fracture length.

2.3 Steady State Flow

If the pressure at any point in the reservoir system is constant (independent of time), this flow is considered steady state.

$$\left(\frac{\partial p}{\partial t}\right)_x = 0 \quad \text{..} \quad 9$$

Equation 9 indicates that the pressure change with respect to time at any location x is zero (Bear, 1972). In real reservoir systems, steady state conditions occurs only if production rate remains constant and fluid withdrawal is exactly balanced by fluid entry across the open boundary (i.e. water/CO_2 injection).

2.3.1 Differential Equation

In steady state flow, fluid mass entering the system is equal to the mass of fluid leaving, i.e. the fluid content of porous medium will not changes with time:

Mass In – Mass Out = 0

This is expressed in mass conservation equation:

$$\frac{\partial(\rho\phi)}{\partial t} + \nabla \cdot (\rho u) + q_m = 0 \quad \text{..} \quad 10$$

Equation 10 is a general form of mass conservation for any dimension. The equation describe that the fluid with density ρ flow through a medium with porosity ϕ in the presence of mass sources or sink q_m (Willhite, 1986). If following assumptions are fulfilled:

- Steady state flow

- Single phase flow

- Incompressible fluid

- Isothermal flow

- No mass accumulation

Equation 10 can be simplified to

$$\nabla \cdot u = 0 \dotfill 11$$

Equation 11 is applied, if no sources/sinks, steady state flow, no density change. u is the apparent fluid velocity, which obtained from Darcy's Law for a porous medium:

$$u = -\frac{k}{\mu\phi}\left(\nabla p + \rho g\right) \dotfill 12$$

Substituting darcy velocity u (Equation 12) into mass conservation equation:

$$-\nabla\frac{k}{\mu}\left(\nabla p + \rho g\right) = 0 \dotfill 13$$

If the gravitational force is negligible, fluid flows in 2 dimensions (no z direction) as well as the permeability and the fluid viscosity doesn't change with the time. Equation 13 can be rewritten as:

$$-\nabla\frac{k}{\mu}\left(\nabla p\right) = 0$$

With constant permeability and viscosity:

$$-\frac{k}{\mu}\left(\nabla^2 p\right) = 0 \dotfill 14$$

Equation 14 is the 2-Dimensional differential equation for steady state flow in a porous medium without source or sink. It is used for calculation of pressure distribution in a porous media domain, which is affected by boundary condition, i.e. linear flow, constant pressure for inlet or outlet boundary.

2.3.2 Finite Element Analysis

The finite element method (FEM) has been long known and used in solving partial differential equations in the fields of mechanical engineering. It is a powerful technique applied to reservoir engineering and simulation of fluid within fractured and unfractured porous media (Chen, 2007). To achieve this, the domain over which we wish to compute a variable is being subdivided into so-called finite element.

To solve equation 14, the pressure variation in the domain of interest of the entire element is related to the nodal property through a linear combination as (Peaceman, 1977)

$$\hat{p}(x,t) = \sum_{i=1}^{n} p_i(t)\Phi_i(x) \dots \dots 15$$

Where p is the pressure at node and $\hat{p}$ is the pressure of the entire element, and Φ are the basis functions. The basis functions can be linear, quadratic, cubic or even of higher complexity. The linear basis functions themselves can be evaluated through an easy geometrical relationship, which reduces the complexity towards the equation of a plane:

$$\Phi_i = a_i x + b_i y + c_i \dots \dots 16$$

Where a_i, b_i, c_i are constant values that are different of every node, but can be calculated with above condition of linear variability. The x and y refer to the coordinate position. If a special differential operator L of the following form assumed:

$$\int_V L(\hat{p}) = \nabla \frac{k}{\mu} \nabla^2 \hat{p} + \hat{q} - \phi c_t \frac{\partial \hat{p}}{\partial t} \dots \dots 17$$

The FEM approximation to the solution of pressure is obtained through the following expression

$$\int_V L(\hat{p})\Phi_i dV \to \min \dots \dots 18$$

which is a minimization problem. In the ideal case the above expression would equal zero.

2.4 Analytical Solution with Superposition Principle

Reservoirs exhibit various flow patterns, including linear, radial, spherical flow in idealized form (Barker, 1988).

- Linear flow: Fluids flow occurs through a constant cross-sectional area. (Figure 4a)

- Radial flow: Fluids move towards the cylinder well from all directions.(Figure 4b)

- Spherical flow: Fluid drawn to the partial well across the entire thickness of permeable formation, the trace of flow is like a sphere. (Figure 4c)
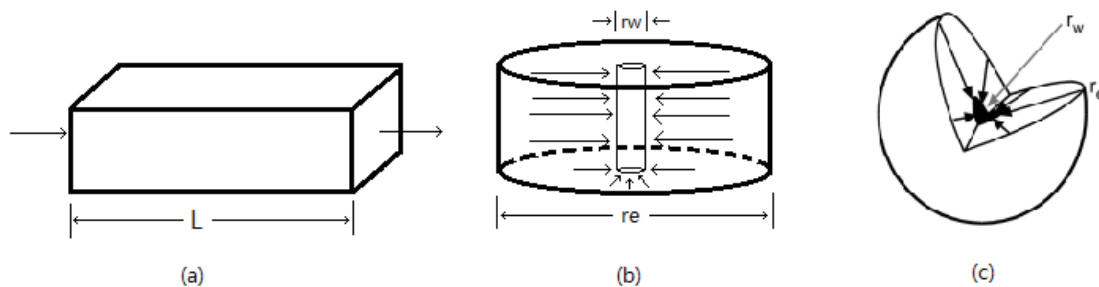
Figure 4: Flow patterns in reservoir, (a) linear flow, (b) radial flow, (c) spherical flow

Multiple-rate, multiple-well problems can be only considered by applying the principle of superposition. When spherical or radial flow is applied for two wells, the principle of superposition must be considered. The mathematical basis for superposition is explained by van Everdingen and Hurst and others (Everdingen, 1949; Shum, 1973)

The superposition principle states that adding solutions of linear differential equation results in a new solution to that differential equation (Earlougher, 1977). In practice, superposition can be applied to find a simplified solution to complex flow problems without t solving the differential equation for different boundary conditions. Superposition can be applied to include more than one well, to change rates, and to impose physical boundaries (Schroeter, 2007).

To illustrate the principle of superposition in space, consider a two-well infinite system in follow Figure 5. Well 1 is an injection well as well as well 2 is a producing

well. Fluid flows from well 1 to well 2, following the pressure gradient. Point 3 is a observation point, which is placed in the center of two wells.
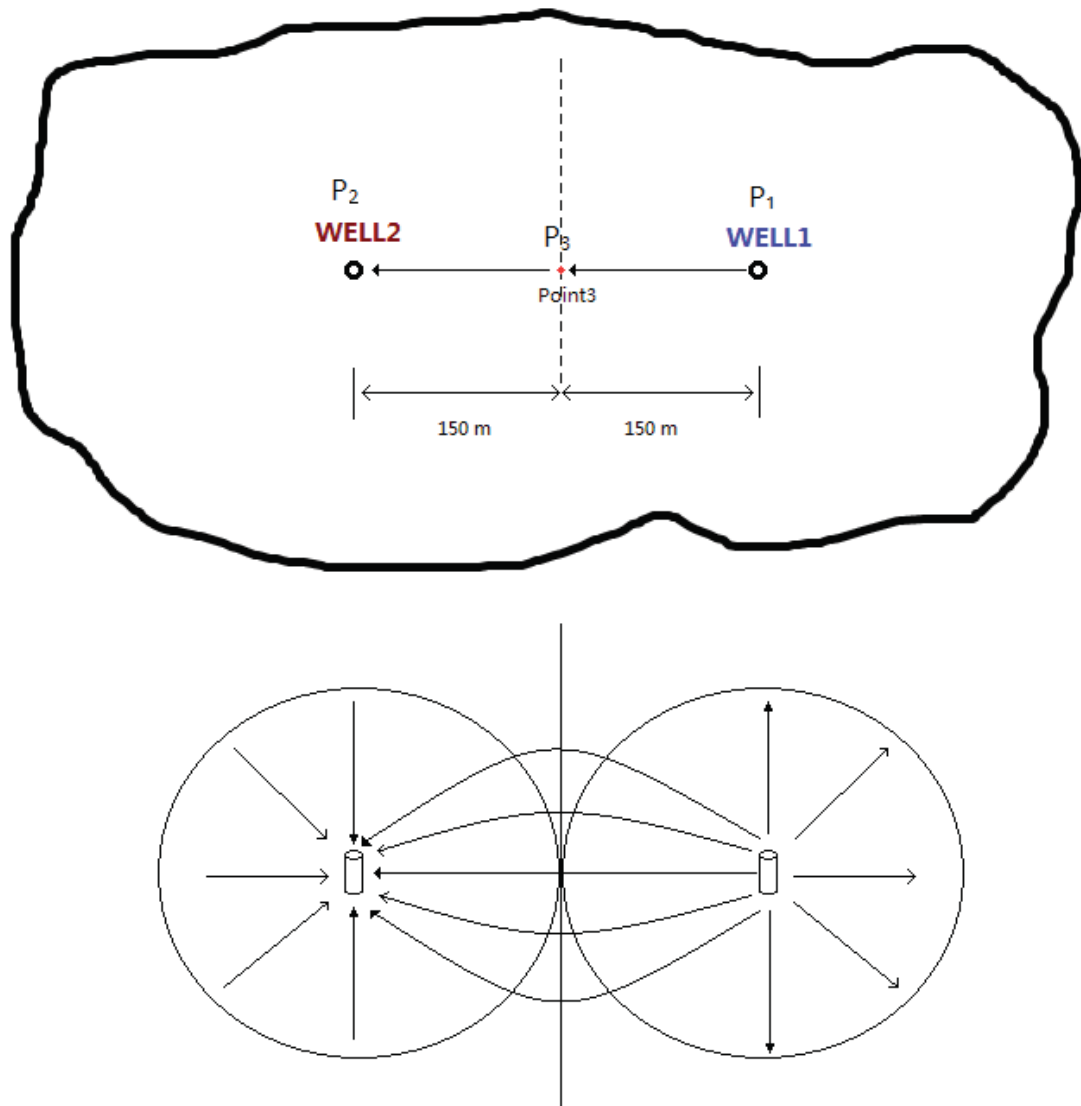
Figure 5: Fluids flow in two-well system from right to left with principle of superposition ($P_1>P_3>P_2$)

If the pressure at point is only affected by well 1 and well 2, It is easy to obtain the pressure at point using the superposition principle. Well 1 injects at rate q_1 and well2 produces at rate q_2, so that pressure at point is sum of pressure at point induced by well1 and pressure at point induced by well 2 (Matthews and Russel, 1967):

pressure at point3= Δp at point3 caused by well1 + Δp at point3 caused by well2

It can be written in simple form as:

$$\Delta P_3 = \Delta P_{3,1} + \Delta P_{3,2}$$

The principle of superposition is applicable for radial flow and spherical flow, when the radius of outer sphere or cylinder is large and the pressure distribution will be affected by long distance of two wells. The larger the radius, the more area fluid will flow through.

2.4.1 Radial Flow Combined with Superposition Principle

For radial flow conditions, the area of cylinder (see Figure 4b) continuously decreases, when the fluid move towards the wellbore. When the flowing fluid approaches the wellbore, the decreasing area causes an increasing velocity of flow, with a corresponding increase in pressure drop. Radial flow for a single well can be derived from Darcy's law equation (Ahmed, 2005):

$$\Delta p = \frac{q_o \mu}{2\pi h k} \ln(\frac{d}{r_w}) \dots\dots\dots\dots\dots\dots\dots\dots\dots 19$$

Symbol	Explanation	Unit
Δp	pressure difference between two wells	Pa
q_0	current fluid flow rate	m^3/sec
μ	fluid viscosity	Pa·s
h	reservoir thickness	m
k	permeability	m^2
r_w	well radius	m
d	distance between wells	m

Equation 19 can be applied to calculate pressure changes surrounding single flowing well. For a multi-well system, combine with superposition, it can be written in following form:

$$\Delta P_3 = \Delta P_{3,1} + \Delta P_{3,2}$$

According to Ahmed (2005), Darcy's law can be rewritten in the form below:

$$\frac{\Delta p}{2} = \frac{q_1 \mu}{2\pi h k} \ln\left(\frac{\frac{d}{2}}{r_w}\right) + \frac{q_2 \mu}{2\pi h k} \ln\left(\frac{\frac{d}{2}}{r_w}\right) \quad \text{.....................................} \quad 20$$

If $q_1 = q_2 = q$, Equation 20 can be changed as follow form:

$$\frac{\Delta p}{2} = \frac{2q\mu}{2\pi h k} \ln\left(\frac{\frac{d}{2}}{r_w}\right) \quad \text{...} \quad 21$$

Solving for permeability, assuming that it is a scalar property:

$$k = \frac{2q\mu}{\pi h \Delta p} \ln\left(\frac{\frac{d}{2}}{r_w}\right) \quad \text{...} \quad 22$$

2.4.2 Spherical Flow Combined with Superposition Principle

In spherical flow, fluids move towards the producing well from all directions (3D), which is different from linear flow and radial flow. Spherical flow is the occurrence of radial flow in both the horizontal and vertical directions (Culham, 1974). When fluid flows spherically towards the well, the pressure is same at any point in dimension, which has same distance to the center of well completion.

Spherical flow for single well can be derivated from Darcy law equation as follow (Hawkins, 1991):

$$\frac{q}{4\pi r^2} = -\frac{k}{\mu}\frac{dp}{dr} \quad\text{... 23}$$

Equation 23 is integrated as:

$$q = -\frac{4\pi k(p_e - p_w)}{\mu\left[\dfrac{1}{r_w} - \dfrac{1}{r_e}\right]} \quad\text{... 24}$$

Where, r_e: radius of large sphere;

r_w: radius of small sphere;

p_e: pressure at large sphere;

p_w: pressure at small sphere;

q: fluid flow rate from large sphere to small sphere;

The integrated flow equation (Equation 24) can be applied for predicting steady-state flow of incompressible fluids. Spherical flow may occur in wells that do not penetrate the entire formation, when completion length is small compared to formation height.

For two-well problems, spherical flow can be expressed using the principle of superposition:

$$\Delta P_3 = \Delta P_{3,1} + \Delta P_{3,2}$$

$$\Delta P_3 = \left(\frac{q_1\mu}{4\pi k}\left(\frac{1}{\frac{l_w}{2}} - \frac{1}{\frac{d}{2}}\right)\right) + \left(\frac{q_2\mu}{4\pi k}\left(\frac{1}{\frac{l_w}{2}} - \frac{1}{\frac{d}{2}}\right)\right)$$

$$\Delta P_3 = \frac{(q_1 + q_2)\mu}{4\pi k}\left(\frac{1}{\frac{l_w}{2}} - \frac{1}{\frac{d}{2}}\right) \quad\text{... 25}$$

Where, l_w: partial completion well length, m;

d: distance between two wells, m;

In this case, $q_1=q_2$, only the fluid flow direction is reversed. Equation 25 can be rearranged to calculate permeability from ΔP:

$$k = \frac{(2q)\mu}{4\pi\Delta P_3}\left(\frac{1}{\frac{l_w}{2}} - \frac{1}{\frac{d}{2}}\right) \quad\text{...} \quad 26$$
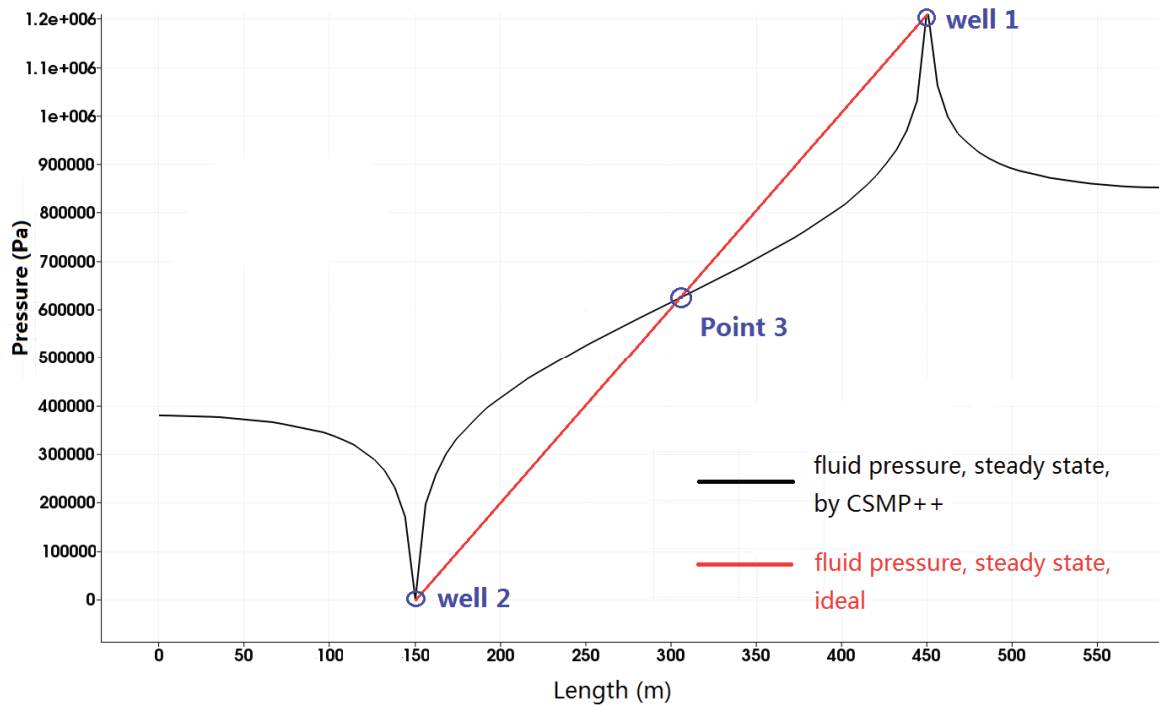
Figure 6: Pressure distribution of steady state between two wells in linear relationship

Because of location of point 3, ΔP_3 is half ΔP (linear relationship, see Figure 6), which between well 1 and well 2. ΔP can be obtained from FEM simulation, so that permeability is solved by:

$$k = \frac{2q\mu}{\pi\Delta P}\left(\frac{1}{l_w} - \frac{1}{d}\right) \quad\text{..}\quad 27$$

2.5 FEM Analysis of Permeability of DFM using CSMP++

Effective permeability can be estimated by using finite element method. Fracture permeability can be calculated, when the aperture is known:

$$k_f = \frac{b^2}{12}$$ 28

Where b is aperture size of fracture with the unit of m. Then, Darcy's flux is computed by solving for steady state fluid pressure with fracture and matrix. The fluid volume source q can be solved by AMG solution based on FEM, when the pressure difference is fixed. Boundary conditions during the flow simulation are imposed. The flux-integrated permeability from the fracture-matrix system at a prescribed pressure gradient can be estimated under the total fluid flow rate which is given by FEM (see Figure 7). For single-phase flow, effective permeability can be written as below:

$$k_{eff} = \frac{q\mu L}{A\left(p_f(u) - p_f(d)\right)}$$ 29

where $p_f(u) - p_f(d)$ = fluid difference pressure applied to inlet and outlet boundaries, Pa;

A = cross-sectional area of boundary perpendicular to flow, m²;

q = Fluid volume source through model, m/s;

L = Length of model in direction of flow, m;

The flux through the Dirichlet boundaries is integrated over the area A of these surfaces. The result will be more accurate by utilization of complementary FE discretization of the model.
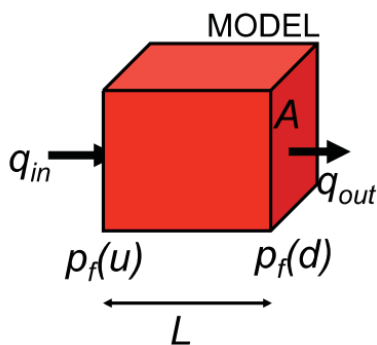
Input Parameter	Output Pramter
Matrix Permeability	
Well Permeability	Fluid pressure of injection well or inlet boundary
Fluid volume source	
Fluid pressure of producing well or outlet boundary	
Fluid viscocity	

Figure 7: Illustration of the effective permeability computation approach (Matthai, 2008)

The matrix permeability, fluid volume source and fluid pressures are input parameters for the CSMP++ Simulation. The boundary condition contains the

pressure of outlet boundary and flow rate through the whole box. After simulation, pressure difference between two wells or boundaries as a result returns from the simulator (see Figure 7). Therefore, effective permeability in the steady state model can be estimated under derivative equation of Darcy's law. Comparing the effective permeability from CSMP++ Simulator with the value in advance fixed, we can know, whether the analytical solution is properly to corresponding steady-state model.

2.6 Discrete Fracture and Matrix Models

A Discrete Fracture and Matrix model (DFM), which is based on the concept of discrete fracture network (DFN) is mainly used for heterogeneous and fractured rock masses (Carlson, 1993). The DFM approach models geometry of the fracture network explicitly. The approach consists of three general steps:

1. Analysis of fracture data, i.e. fracture size, fracture orientation;

2. Generation of discrete fracture networks, based on result of fracture data analysis;

3. Analysis of discrete fracture network, i.e. complex multiple flow simulation;

Since the complex behavior of flow and transport in naturally fractured reservoir is commonly not captured sufficiently by conventional simulation, discrete fracture and matrix simulation techniques have been developed. DFM techniques reduce the dimensionality of the fractures, representing them as lines in 2D or surfaces in 3D.
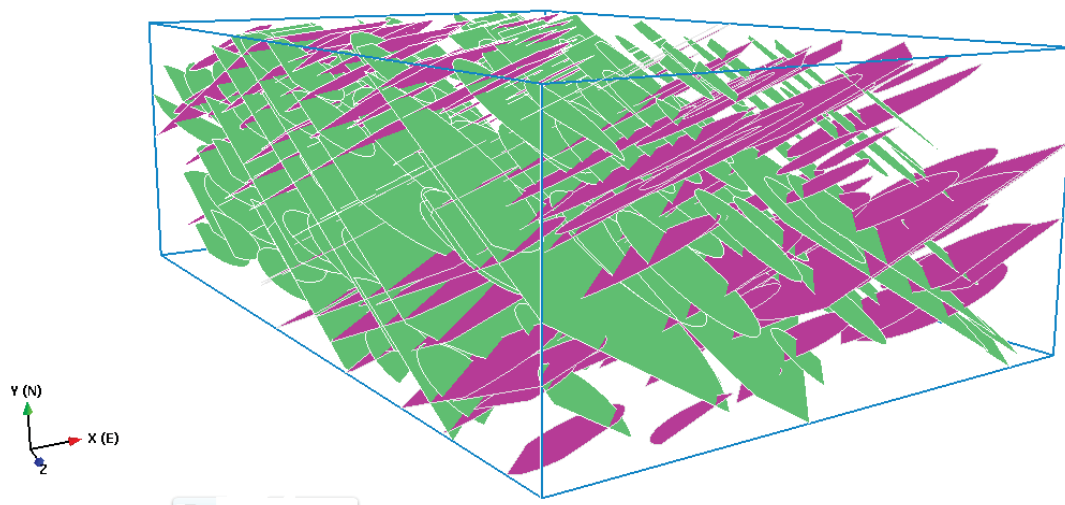
Figure 8: A simple Discrete Fracture and Matrix model

Figure 8 illustrates a simple DFM model consisting of two sets of fractures (green and purple) with different orientation. The model handles both 2D and 3D systems and includes fracture-fracture, matrix-fracture and matrix-matrix connections. It offers numerous advantages over conventional models, including:

- More realistic representation of fracture network geometry;

- Direct simulation of reservoir connectivity, relative efficient computation;

- no longer necessary to compute effective permeability for sub-grid scale fractures;

A fracture is any local discontinuity plane in a geologic formation. Fractures can provide permeability for fluid flow and transport. The fractures system in DFN approach is mainly described by (Boris, 1986):

- Fracture intensity;

- Fracture size;

- Fracture orientation;

- Fracture shape;

Fracture intensity:

Also called fracture density, is the amount of fractures per unit volume or per unit area. Four measurements for fracture intensity exist (Dershowitz, 1992):

Total number of fractures;

P10: Number of fractures per unit well length;

P21: Total fracture length per unit area;

P32: Fracture area per unit volume of rock;

P33: Fracture volume per unit volume of rock;

Fracture size distribution:

Power law distribution is often used to describe the frequency distribution of fracture size. Obeying a power law distribution, characteristic length scales are absent in the fracture growth process (Mourzenko, 2001). The absence of other characteristic length scales result to propose a simple formulation for the fracture length:

$$\frac{dl}{dt} \approx l^a \qquad \text{... 30}$$

When a population of nuclei of different length exists in a system, a power law length distribution will be applied by simple generation model with an exponent –a.

Trento (1996) has shown that the length L and aperture b of fractures follow power-law distribution over various length scales:

$$N = m \cdot L^{-a} \qquad \text{... 31}$$

Where N is the cumulative number of Factures in a given sample with length equal or greater than L. The exponent a and empirical factor m depend on the particular formation. When the exponent a is smaller than 3, the fractures appear more numerous and larger as the size of the region increases. Equation 31 contains no characteristic length scale, so that the consequence of power law distributions is very important. The power law distribution is a straight line on a log-log plot. Figure 9

shows the power law distribution for the general length of microfracture (0.001mm-0.1m) and macrofracture (>10 m) in log-log plot.
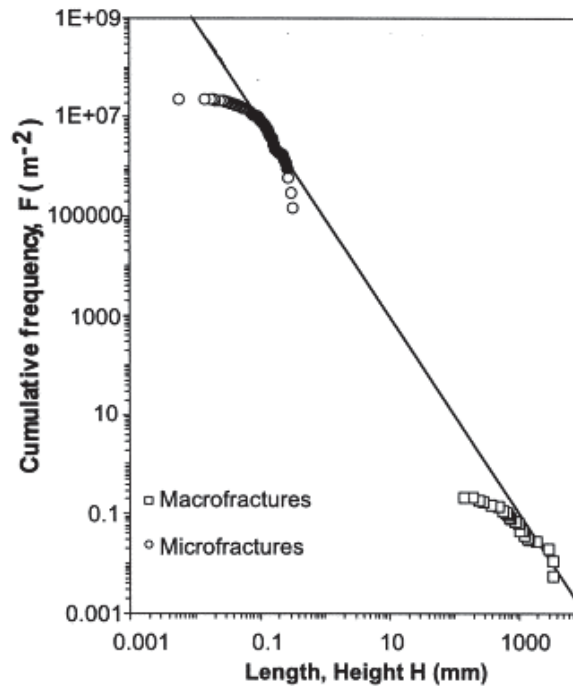
Figure 9: Power-law distribution for microfracture and macrofracture length (Trenton, 1996).

The frequent occurrence of power law distribution may arise because of the intrinsic heterogeneity of Earth materials. Certainly, power law is not the only possible distribution found in natural fracture system. Other distributions that have also been used include log normal, gamma and exponential law. However, power law distribution is dominated in heterogeneous system. The key argument, that power law distributions are popular used for fracture size distribution, is the absence of a characteristic length scale in the fracture growth process (Bonnet, 2001).

Fracture orientation:

Fracture orientation gives the direction and incline of fractures (Knott, 1976). Two important parameters, trend and plunge (referring to linear features) determine the fracture orientation. Trend refers to the positive angle from the North axis and plunge is the positive angle measured downward from the horizontal. Fracture orientation can be measured as either pole or dip vectors (refer to planar features). A pole vector

is a vector normal to the mean fracture, whereas a dip vector is the longest vector tangent to the fracture plane (see Figure 10).
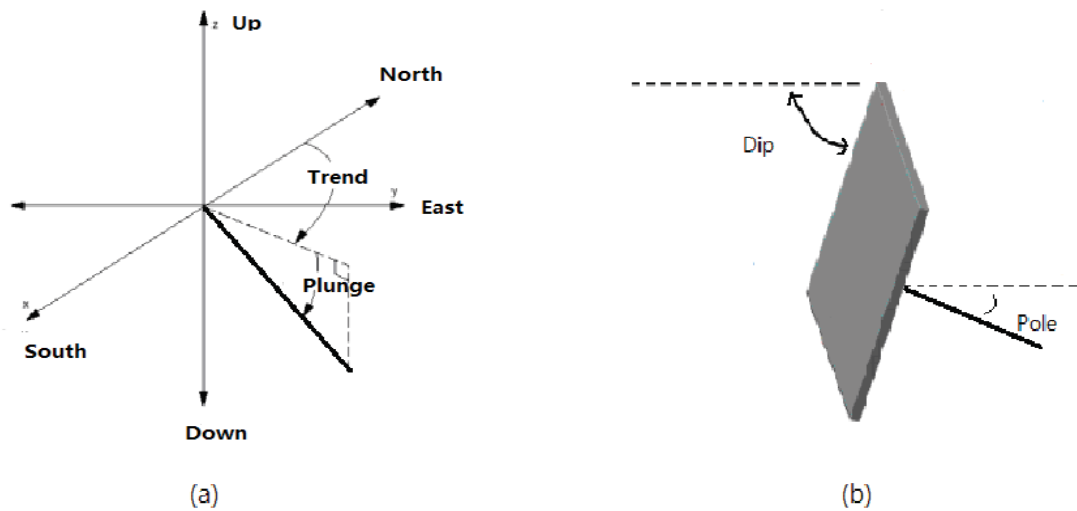
Figure 10: Illustration of vector of fracture orientation, (a) linear feature, (b) planar feature

Fractures with similar orientation can be grouped to a fracture set. Such individual fracture set is similar to fracture generating processes, due to identified states of stress.

Fracture shape:

In reality, fractures are caused by varies strength of earth stress in different directions, so that they exist as planer of varies form. However in DFM models, generally a single fracture is a representative polygon, which may be disc-shaped for higher edge counts.

2.7 Simulation Process

The analysis of the mathematical model of steady state is to solve a linear equation, including internal and external flow equations and boundary conditions. For a homogeneous well test model, the exact solution is obtained through the analytical method. With the analytical method, we can accurately calculate pressure difference any time and any place. Simple analytical solutions for well test models are easy to use. To simulate fluids in naturally occurring reservoirs containing complex boundary conditions, inhomogeneous layers or multiphase flows, numerical methods such as

Finite Element Analysis can be applied. Users of numerical methods have to consider that only approximate solutions are provided by the simulator.

This section will present the procedure of numerical method, which solves the pressure problem compared to analytical methods.
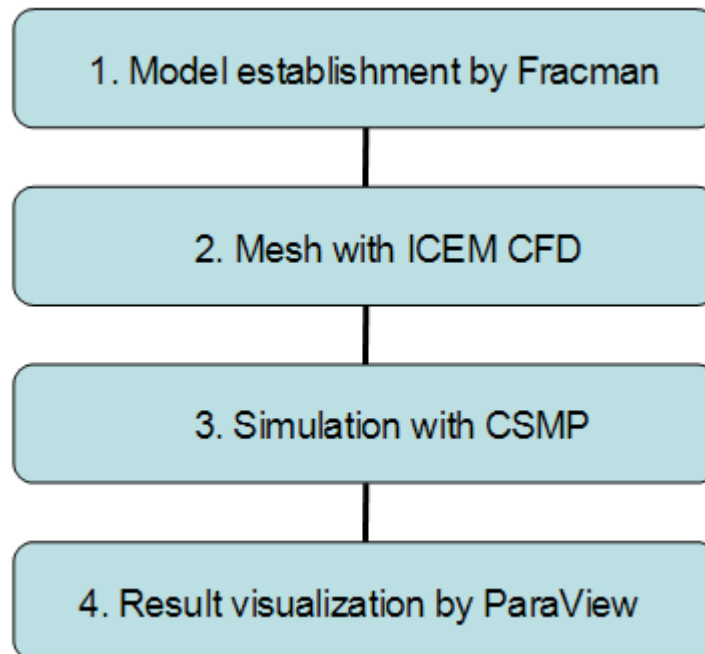
Figure 11: Flow chart of numerical solution for steady state flow

Figure 11 shows the flow chart for numerical methods for steady state flow. The first step is to create models by software. In matrix-only based models, the pressure distribution of the reservoir can be simulated by numerical and analytical simulators. Furthermore, numerical solution can solve the complex case, such as DFM models. Models can be created in different form based on different fracture properties (orientation, size, intensity). Prior using simulators such as CSMP++, the important procedure is that models are meshed in fine elements by ICEM CFD. The accuracy of results in CSMP++ mainly depends on the size of meshing element. After meshing, some essential parameters of models are input to configuration file of CSMP++ and then run the CSMP++ to get the solutions. The CSMP++ can output the results in logs file. It's not directly perceived through the senses. An application (ParaView) can convert the logs date to directly visualization in 2D or 3D. It can analyze the data from CSMP++ conveniently and directly.

2.7.1 Models Setup

Two model groups are created and simulated in this part of thesis. The models need be big enough, so that the pressure perturbation will not affect the result of simulation. The first group is modeled without fractures (Matrix-only models) and contains boundaries and wells. Both simulators (analytical and numerical) using this model group will present pressure and permeability as a result. After the simulation process, the results of both methods are be compared.

Wells are composed of one injection well and producing well, which has same flow rate of injection well. Boundaries are composed of Inlet and Outlet boundary, that fluids flow into inlet boundary and out of outlet boundary with same flow rate as wells. However, because surface area of them is different, the fluid volume sources (fluid velocity) are different, which is paid special attention to configuration file of CSMP++. In this group model, equivalent permeability in this group model is considered as the permeability of matrix.

The second group is models with fractures and boundaries/wells (DFM models). The well or boundary condition is same as first group. Moreover, two fracture sets are present in each of these models with diverse orientation, size and intensity. in this group model, equivalent permeability is considered as both permeability of matrix and permeability of fractures simultaneously.

For each model group, we have also conducted three simulations differing in their setup:

1. Without wells. Fluid flows as linear flow through Inlet to Outlet boundary.

2. With fully penetration well completion. Flow trace is like radial flow from injection well to producing well (matrix-only model).

3. With arbitrary completion length. Flow trace is like sphere flow from injection well to producing well. (matrix-only model)

2.7.1.1 Model Discretization

An analytical solution for the pressure distribution in a complex structurally model (e.g. contain fractures, matrix and wells) is difficult to achieve. This is the reason that numerical methods and partial differential equations is essential to be applied. The

numerical solution provides an approximated solution and it can simulate such reservoirs with certain accuracy. Model discretization is the first step of numerical methods. It divides a continuous domain into a finite number of discrete parts while keeping a proper representation. we will not go into detail, how to mesh the models with CFD software. However, the selection of mesh size in CFD software will affect the result. This will be discussed in section 2.7.2.
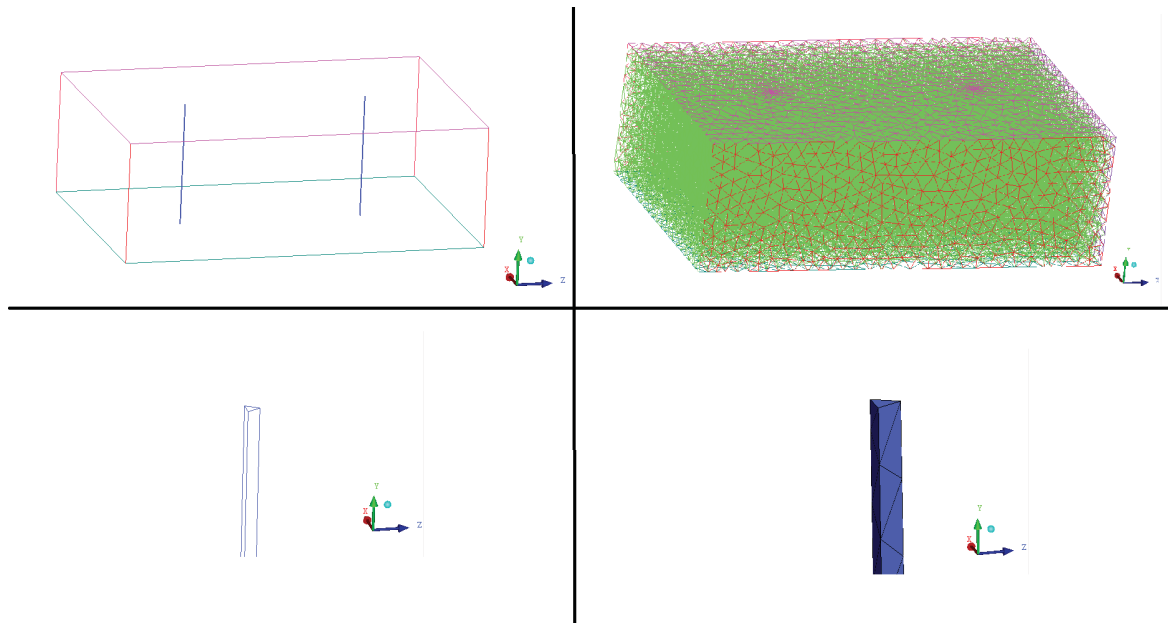
Figure 12: Discretization of wells and matrix in space (left hand: continuous model and wells; right hand: discretization of model and well)

Figure 12 shows the transformation from a continuous model with wells to discretization. The right hand side shows "mesh", which consists of a finite number of cells. We can form our domain with an arrangement of grid blocks or a derangement of grid blocks. However, the properties of each block grid are constant. Therefore, for each cell, there's only one fixed value for porosity, permeability, and others. So we can break down a complex structure into amounts of individual cells and compute their interaction numerically.

2.7.1.2 Matrix-Only Models

Matrix-only models are used to verify the numerical methods. Models are simply and no fracture existence. Fluids are simulated from right well or boundary to left well or boundary flow. For with well case, wells are placed in the region of model. One well is injection well, the other is producing well. The radius of both wells are equal.

The injection rate is equal to production rate with inverse direction. The other parameter for model and simulation as follow:

Table 1: General parameters for matrix-only models

Size of region-box	600*400*200 m
Well shape	Triangular
Side length	1 m
Well size	0.433 m^2
Distance between two wells	300 m
Injection rate	100 m^3/day
Producing rate	-100 m^3/day
Viscosity	10^{-3} Pa·s
Density	1000 kg/m^3
Initial pressure for production	0 Pa
Permeability of matrix	1.0E-14 m^2
Permeability of wells	1.0E-8 m^2

In the establishment of the numerical model, the cross section of well is not circular. It is described as a regular triangle in order to be easily meshed in ANSYS CFD. The surface of both models, which the fluid flow through, is not the same as analytical solution. Therefore, the precision of the model is discussed below.

For the well of the numerical model, each side length of triangle is set as 1 m. As a result, the radius of internally tangent circle is equal to 0.289 m. The radius of externally tangent circle is equal to 0.577 m. The radius of internally tangent circle is taken as the radius of the well for analytical solution. The pressure difference can be calculated by numerical methods firstly with 1 m side length of triangle well and then analytical methods estimate the pressure difference with 0.289 m well radius. The surface area of well and pressure differences are compared as below:

Table 2: Comparison of pressure difference for both models, well radius=0.289 m for analytical solution

	Numerical model	Analytical model	Difference
Surface area of well	600 m^2	363 m^2	39.5%
ΔP	129189 Pa	127950 Pa	0.96%

Table 2 states that there is a difference of 39.5% in well surface area. The pressure difference in analytical model is 0.96% less than in numerical model. Now it can be assumed, if the surface area of well in both models are equal. The well radius can be set 0.477 m in analytical method for this assumption. Thus, the surface area s of both wells are nearly equal. The comparison of pressure difference:

Table 3: Comparison of pressure difference for both models, well radius=0.477 m

	Numerical model	Analytical model	Difference
Surface area of well	600 m^2	599.7 m^2	0.05%
ΔP	129189 Pa	118703 Pa	8.12%

Table 3 states that there is a difference of 8.12% in pressure difference, although the surface area of well are nearly equal. Therefore, the internally tangent circle of triangle is selected as the well radius for analytical model. The detailed calculation process and monitor-file for Table 2 and Table 3 are provided by Appendix A.

2.7.1.3 DFM Models

In real naturally fractured reservoir, fractures are existed in different orientation, intensity and size. We need create geological models with various fracture properties, which could better represent the actual geological system. 8 DFM models with various fracture characteristics are created in a region-box of 600x400x200 m, which is the same as Matrix-only models. Except for fractures related parameters, others parameter for DFM models are also the same as matrix-only models (i.e. viscosity, porosity, well size).

Table 4: General properties for the fracture system in DFM models

Model	Enhanced Baecher
Fracture Intensity	P32 (fracture area/ region volume)
Fracture Orientation	Constant, Pole
Fracture Size	Power law distribution
Min. X value	26 (model1-4)
Exponent	2.85 (model 1-4)
Fracture Shape	Disk
Fracture Aperture	0.001 m
Fracture Permeability	8.33e-11 m

Model 1-4 have variable fracture intensity, trend, plunge, and truncation. Model 5-8 are similar to model 1-4 having same intensity. In Appendix B, the fracture properties of model are shown in detail. Every model has two fracture sets and because of different fracture intensity, the number of fracture in model is also different. The fracture size distribution is following power laws for all models (see Table 4). Model 5-8 with increasing X_{min} and exponent, the fracture intensity keeps constant for all. Trend and plunger are respectively corresponding to model 1-4. The truncate of fracture size distribution is below 300 for all DFM models, that the maximum fracture size will not above the distance between two wells (or two boundaries).

In all models, the fracture intensity is defined as P32 (fracture area per unit volume), the interval is between 0.03 and 0.7, and thus the total fracture count is between 300 and 600. The fracture size follows power law distribution, there're two important parameters, minimum x and exponent. The minimum x (minimum length of fracture) will be set as 26 m for model 1-4, which dominate the distribution of fracture size. The maximal fracture size is controlled by the maximal value of truncation, which in model1&2 is 150m, in model3&4 is 300m and in model 5-8 is 200m. The exponent is set as 2.85 in models 1-4. The value for exponent and minimum x will be set progressively increasing in models 5-8. Different minimum x and exponent will affect the fracture size distribution. Detailed Charts of Fracture size vs. frequency are provided by Appendix C. An overview of all models in fracture modeling software is provided by Appendix D.

If all fractures extend across the region of interest, the single largest fracture controls the permeability of the region, and effective permeability increases as the size of the region increases (Rossen, 2000). The largest fracture size is control by Max. Truncate from power law distribution. The length of largest fracture is assumed below the distance of two wells or two boundaries in all models. Therefore, the permeability will not affected by the largest fracture.

Above 8 DFM is with a certain condition that the wells always penetrate the fractures (P10 >0). In reality, when the partial penetrating well is short, it is possible that wells intersect no fracture (P10=0). We have to consider, whether it will affect effective permeability, when P10=0. Based on original model 5-8, Model 5b-8b are modified models for partial penetration well,that wells intersect no fracture in those models.

2.7.2 Comparison of Matrix-only Models with Analytical Solution

In this subsection, verification of numerical methods are discussed. Because It is not the proper way to implement analytical solution for complex structural system (i.e. include fractures, wells and matrix at same time). Matrix-only model are used as numerical model, which also can be solved by analytical method. There're two wells or two boundaries in the model, which fluid will flow through them. The setup of this verification case with a homogeneous, isotropic simulation model is as follow: The first well is an injector with a constant flow rate; but the bottom-hole pressure is unknown. The second well is a producer, whose bottom-hole pressure is assumed to be zero. We input the flow rate of injection well and the Dirichlet pressure of production well into the CSMP++ based FEM pressure diffusion model. The simulation determines pressure of injection well is given by CSMP++. This pressure is used into the corresponding Darcy's law equation (radial flow, sphere flow, linear flow) to calculate the effective permeability from the analytical equation. In the simulation, the permeability is used as an input parameter. The value can be compared with the effective permeability to assess the accuracy of the estimation model. If the fractures exist, it is not the proper way to calculate the effective permeability from an analytical solution. For this we will employ the verified FEM pressure diffusion model.
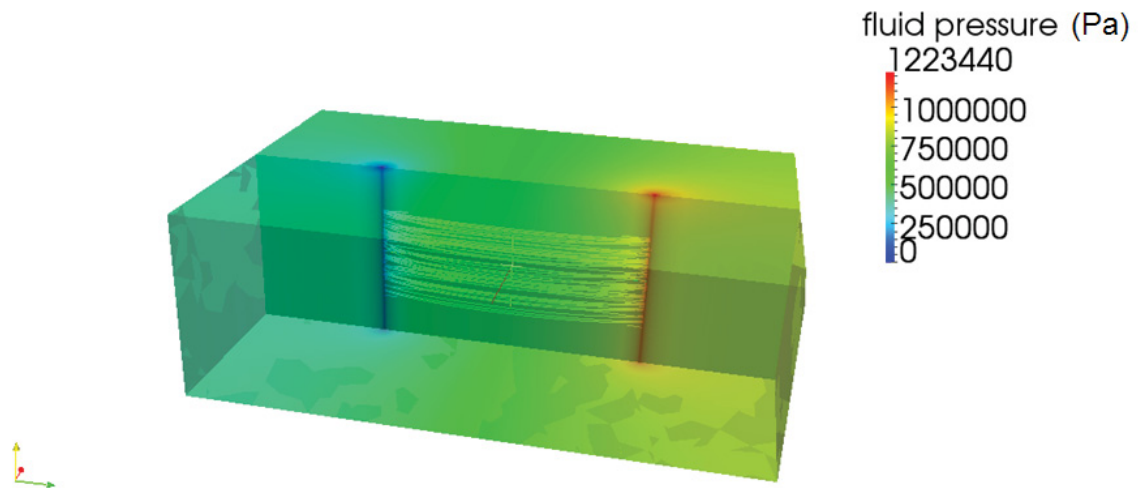
Figure 13: Visualization of pressure distribution and streamline tracing between two fully penetrating wells (Model 1, radial flow)
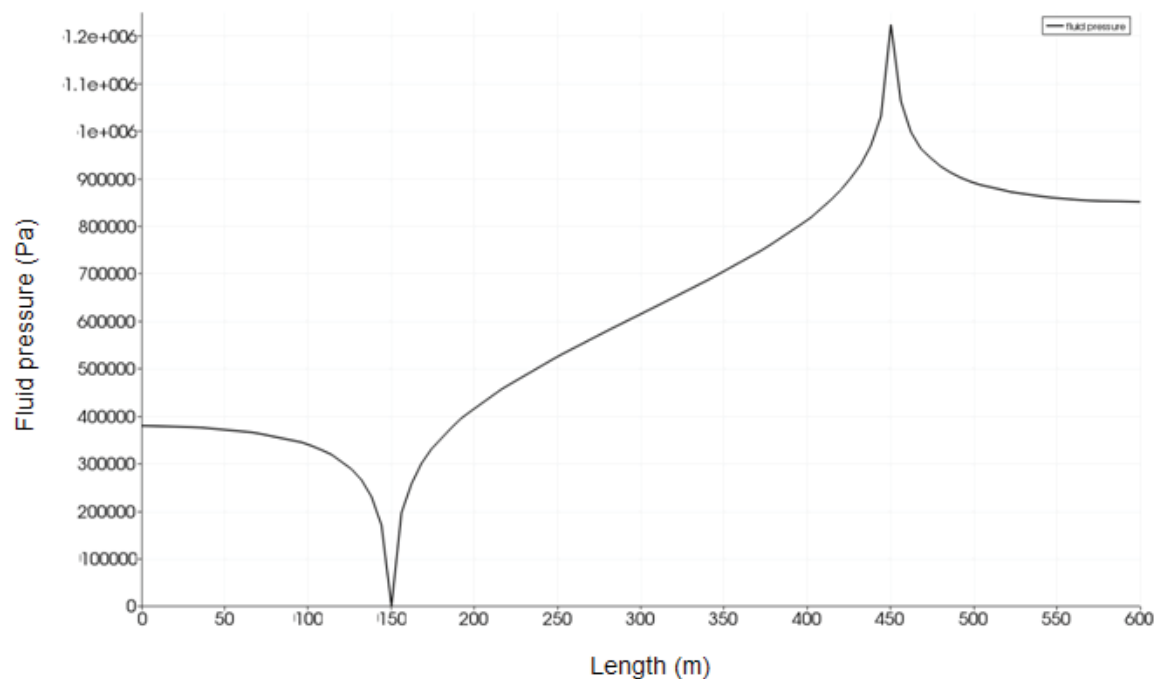
Figure 14: Inter-well pressure profile (model 1)

The Streamline of fluids in Figure 13 is presented by visualization software "ParaView". The flow path between the two wells is exactly as predicted by the radial flow in analytical solution (Figure 5). Figure 14 shows that pressure drops from the injection well (highest) to producing well (lowest) are as a smooth curve.
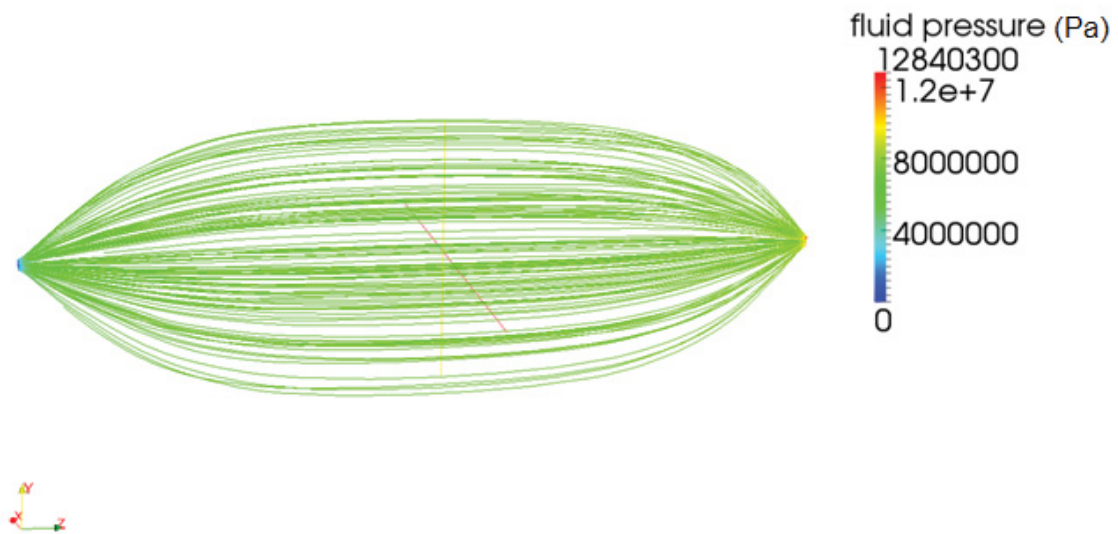
Figure 15: Visualization of streamline between two partial penetrating wells (Model 2, sphere flow)
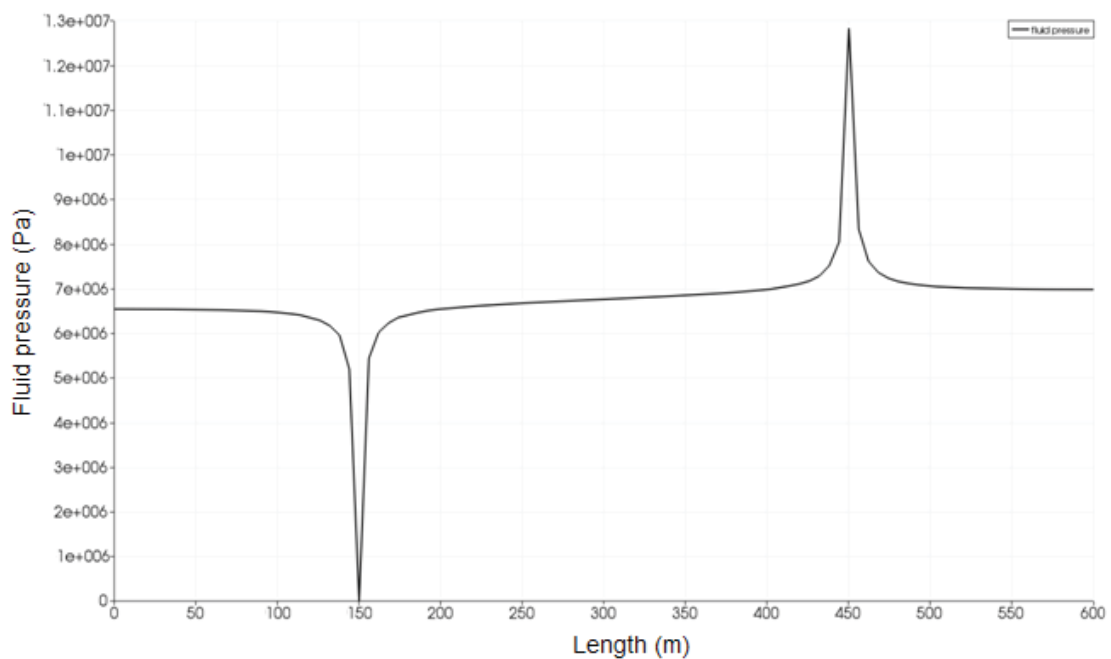
Figure 16: Inter-well pressure profile (model 2)

Figure 15 shows streamline between two wells for spherical flow in numerical solution. It is quite different from that for radial flow. Fluids flow from injection well to producing well as sphere in dimensions. The pressure distribution in Figure 16 shows that pressure increases or decreases rapidly near the wells.
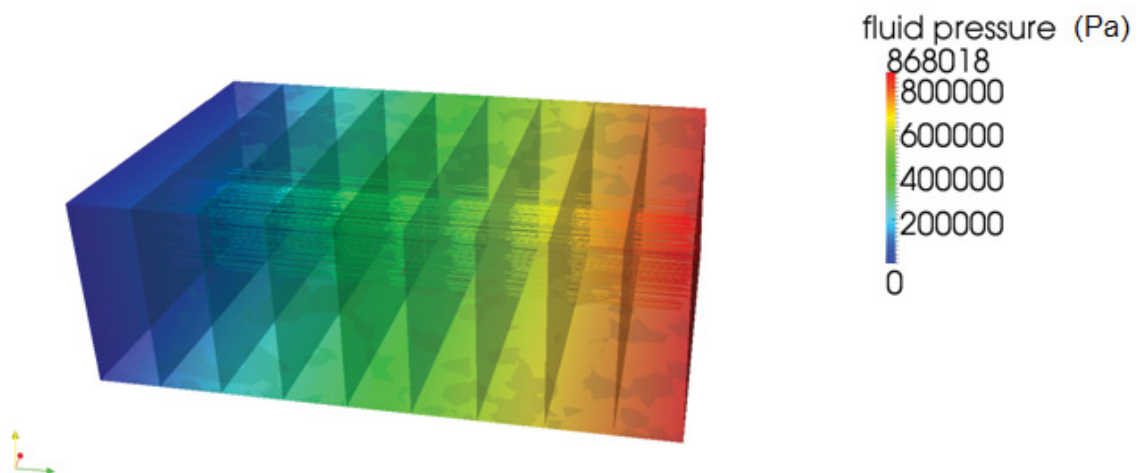
Figure 17: Visualization of pressure distribution and streamline between two boundaries (Model 3, linear flow)
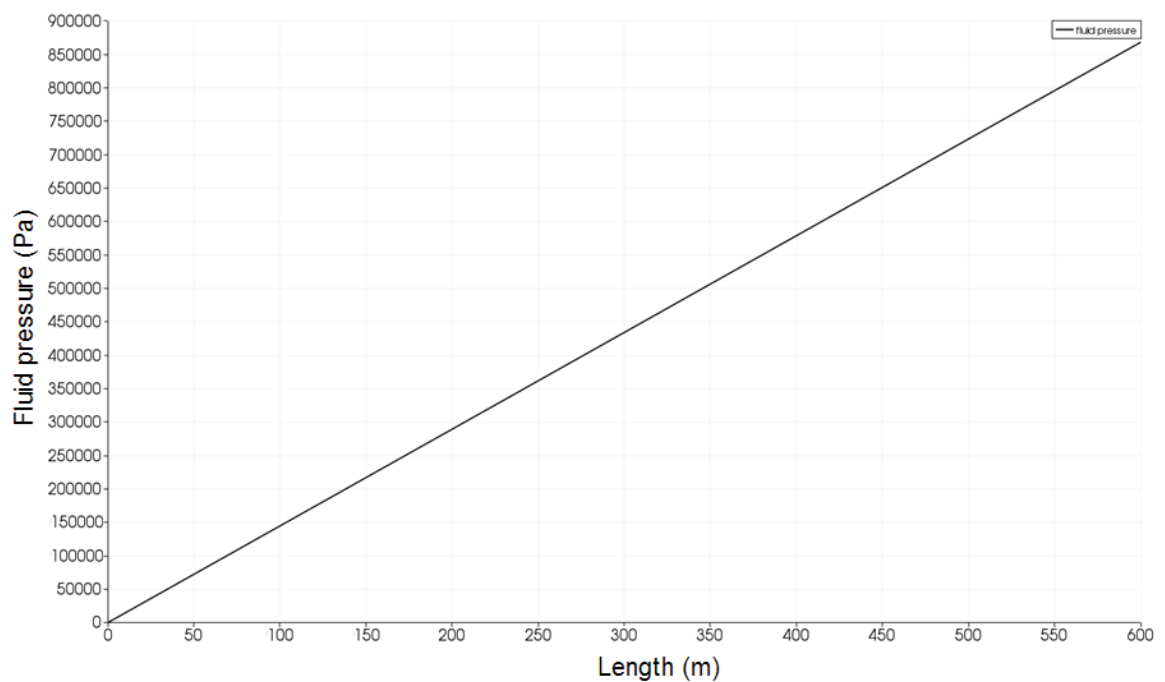
Figure 18: Inter-boundary pressure profile (model 3)

Figure 17 shows the pressure distribution and streamline between two boundaries. Fluids flow straightly from inlet boundary to outlet boundary. The pressure between two boundaries drops progressively. Pressure distribution in Figure 18 exhibits a straight line, which is corresponding to linear flow in steady state with analytical solution.

The wellbore pressure for injection well with a fixed flow rate can be solved by using FEM analysis based on CSMP++. We replace this pressure solved by numerical method (max. element size = 20m) into the pressure in converted Darcy's law equation (Equation 2, Equation 22, Equation 27) and use other parameter as same as numerical method (i.e. flow rate, viscosity, penetration length). Accordingly, we can solve the equivalent permeability from Analytical solution.

Table 5: Effective permeability calculated with analytical solution by using pressure solved in FEM analysis

	Well penetrating length	ΔP from FEM analysis (Pa)	superposition	k_{eff} (calculated from analytical solution)
1	Fully penetration (radial flow)	1.22E+06	x	1.04E-14
2	Partial penetration (sphere flow)	1.38E+07	x	1.05E-14
3	Box-model (linear flow)	8.68E+05		1.00E-14

The permeability of matrix as 1.0E-14 m^2 and permeability of well is used as 1.0E-8 m^2 in numerical models (matrix-only and DFM). Table 5 states that the effective permeability calculated with analytical solution is about the same as the one used in the numerical simulations. It is a little greater than the permeability of matrix for fully and partial penetration well case, because the wells have a large permeability. Analytical solution considers them as an equivalent permeability.

Table 6: Comparison of parameters in analytical solution and in numerical solution

	Analytical solution	**Numerical solution**
Method	Darcy's law	FEM analysis
well shape	circle, r_w=0.289 m	triangular, side length=1 m
flow rate (q)	100 m^3/d	
viscosity (μ)	1000 Pa·s	
matrix permeability (k)	1.0E-14 m^2	
full penetration length (l)	200 m	
partial penetration length (l_w)	5 m	
well distance (d)	300 m	

We also can compare the pressure solved by analytical solution and numerical solution directly: pressure calculated by Darcy's law in analytical solution and pressure estimated by FEM analysis in numerical solution. All the input parameter is same, except for well shape (see Table 6). In analytical solution, the well is considered as a circle. In numerical solution, the well is represented as a triangular that is easy to mesh. In section 2.7.1.2 we have discussed the value of well radius corresponding to a fixed side length of triangular. However, not only input parameters, but also the degree of model precision will affect the result. The primary factor is maximum element size for meshing process.

In previous sub-section, we discuss the model discretization briefly. During the meshing process, I find that it's quite important to select an appropriate value for mesh size. It will directly affect the simulation result. We use 20 m as the maximum element size (cell size) for model verification (permeability comparison). It obtains an acceptable result. Next, we use 40 m as the maximum element size and check the accuracy for simulation result.

Table 7: Comparison of max. element size with 20m and 40m to analytical model

Well penetration	Fully	Partial	No well
Flow pattern	Radial	spherical	linear
Δp analytical (Pa)	1.152E+06	1.449E+07	8.681E+05
Δp numerical (20m)	1.223E+06	1.376E+07	8.680E+05
Accuracy (mesh=20m)	4.47%	5.0%	0.004%
Δp numerical (40m)	1.232E+06	1.284E+07	8.681E+05
Accuracy (mesh=40m)	6.5%	12.86%	0.01%

Table 7 shows the resulting pressures estimated by the analytical solution and matrix-only numerical simulations (20 m and 40 m). The accuracy of each matrix-only model comparing to analytical methods are shown above (detailed calculation refer s to Appendix E). We can find, that the model with smaller value of max. mesh element size will obtain a more accurate result, compared to analytical method. But during the meshing of models, it takes long time to mesh a fine model (with smaller max. element size). Therefore it is important to choose the appropriate value of max.

element size for meshing. Too large will cause coarse model, that affect the accuracy of simulation. Too small will cost more time in simulation.

3. Results

3.1 Permeability Estimation with Fractures

In this section, 8 fractured models in 2 groups will be simulated by CSMP++, Model 1-4 have diverse fracture intensity, orientation, truncation. Model 5-8 are corresponding to model 1-4 and have same intensity (=0.04).

Model1 (Group 1)

Fracture set	1	2
Fracture Intensity (P32)	0.02	0.02
Trend (degree)	150	120
Plunge (degree)	75	15
Min. Size of Truncate (m)	2	2
Max. Size of Truncate (m)	150	150
Total Fracture number	298	
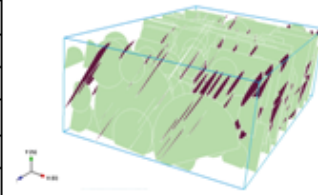
Model 2 (Group 1)

Fracture set	1	2
Fracture Intensity (P32)	0.04	0.035
Trend (degree)	30	160
Plunge (degree)	65	70
Min. Size of Truncate (m)	2	2
Max. Size of Truncate (m)	150	150
Total Fracture number	495	
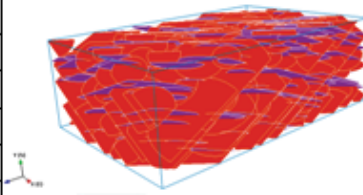
Model 3 (Group 1)

Fracture set	1	2
Fracture Intensity (P32)	0.035	0.04
Trend (degree)	30	160
Plunge (degree)	65	70
Min. Size of Truncate (m)	20	20
Max. Size of Truncate (m)	300	300
Total Fracture number	482	
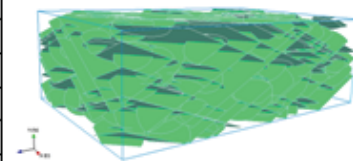
Model 4 (Group 1)

Fracture set	1	2
Fracture Intensity (P32)	0.035	0.04
Trend (degree)	30	160
Plunge (degree)	65	70
Min. Size of Truncate (m)	2	2
Max. Size of Truncate (m)	300	300
Total Fracture number	443	
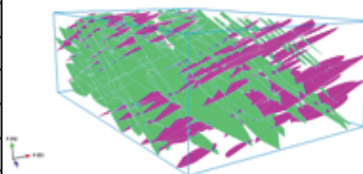
Figure 19: Overview of fracture configuration for Group 1

Model 5 (Group 2)

Fracture set	1	2
Trend (degree)	150	120
Plunge (degree)	75	15
X_{min}	10	10
Exponent	1.5	1.5
Truncate (m)	2-200	2-200
Total Fracture number	500	
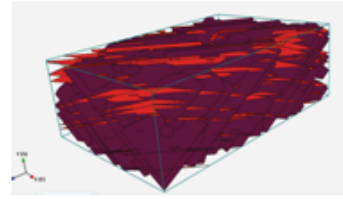
Model 6 (Group 2)

Fracture set	1	2
Trend (degree)	30	160
Plunge (degree)	65	70
X_{min}	20	20
Exponent	1.9	1.9
Truncate (m)	2-200	2-200
Total Fracture number	397	
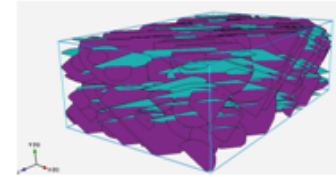
Model 7 (Group 2)

Fracture set	1	2
Trend (degree)	30	160
Plunge (degree)	65	70
X_{min}	30	30
Exponent	2.8	2.8
Truncate (m)	2-200	2-200
Total Fracture number	446	
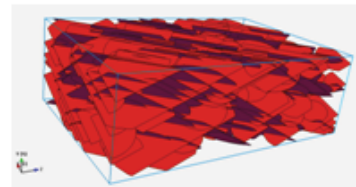
Model 8 (Group 2)

Fracture set	1	2
Trend (degree)	30	160
Plunge (degree)	65	70
X_{min}	40	40
Exponent	3.5	3.5
Truncate (m)	2-200	2-200
Total Fracture number	323	
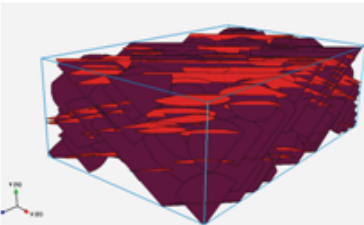
Figure 20: Overview of fracture configuration for Group 2

Figure 19 and Figure 20 show an overview of fracture setup for models of 2 groups. Following 3 sections will indicate these three cases respectively in ParaView only for model 8. Other models are similar, so that they are ignored to show the construction and behavior in ParaView.

3.1.1 Radial Flow
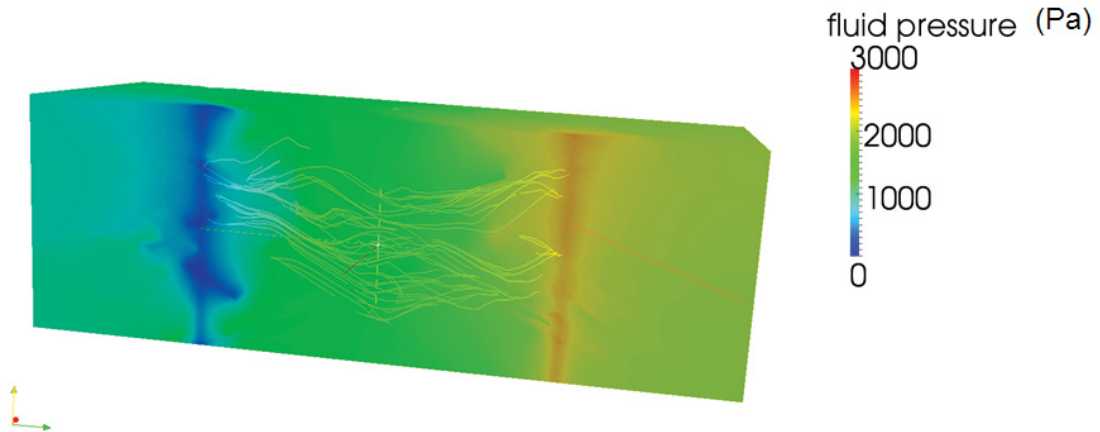
Figure 21: Streamline between two wells (Model 1, full penetration wells)
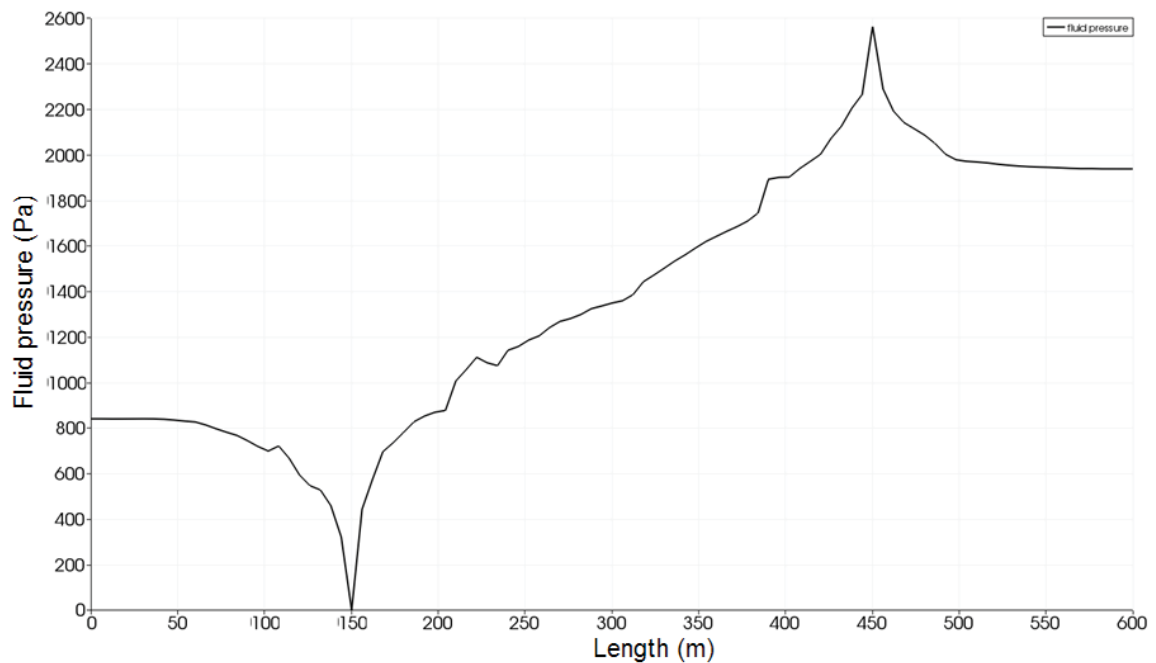
Figure 22: Pressure profile (Model 1, full penetration wells)

Figure 21 shows the streamline for DFM model 1. Because fractures exist, the streamline is irregular as that in only matrix model. Matrix-only model is homogenous, fluids flow as radial flow. However, in DFM models, fluids follow the path of connectivity. Figure 22 shows pressure distribution in DFM model for full well completion. The pressure of producing well is set as 0 for initial condition. The pressure of injection well is calculated by FEM analysis.

3.1.2 Spherical Flow
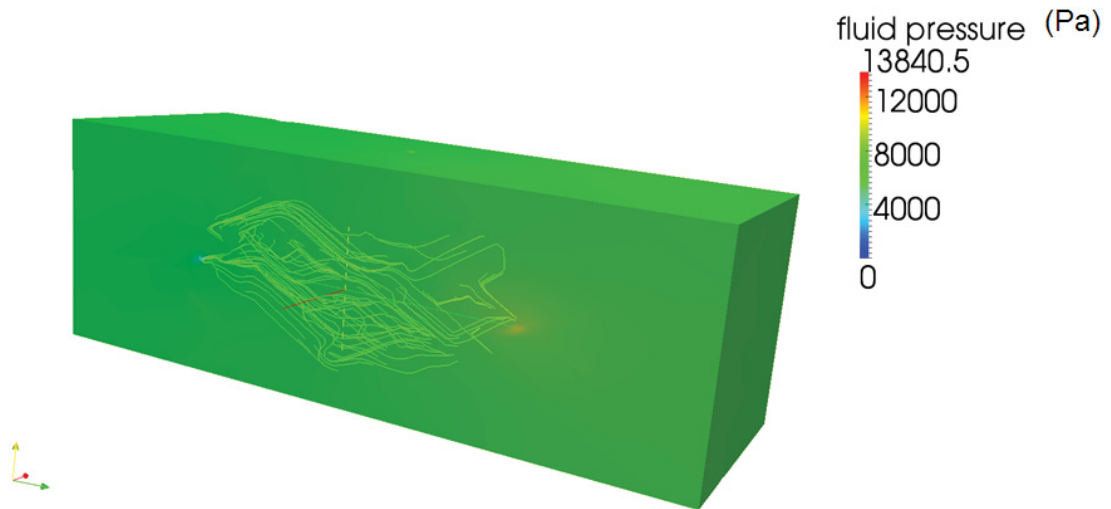
Figure 23: Streamline between two wells (Model 1, partial penetration wells)
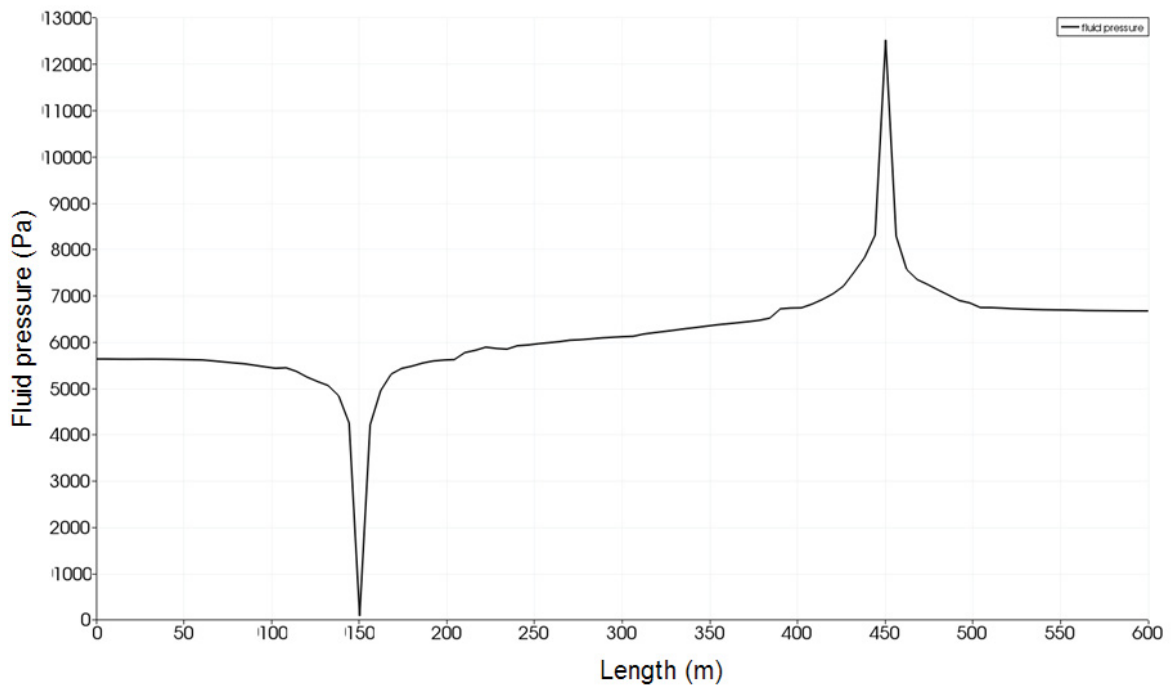
Figure 24: Pressure profile (Model 1, partial penetration wells)

Figure 23 shows that streamline in DFM model for spherical flow. Although the initial condition is same for all models, the area of wells that fluids flow through is different. With the same flow rate, the pressure difference in partial well completion is higher than that in full well completion. Figure 24 shows the pressure drops relative smooth, compared to that in the model only with matrix.

3.1.3 Linear Flow
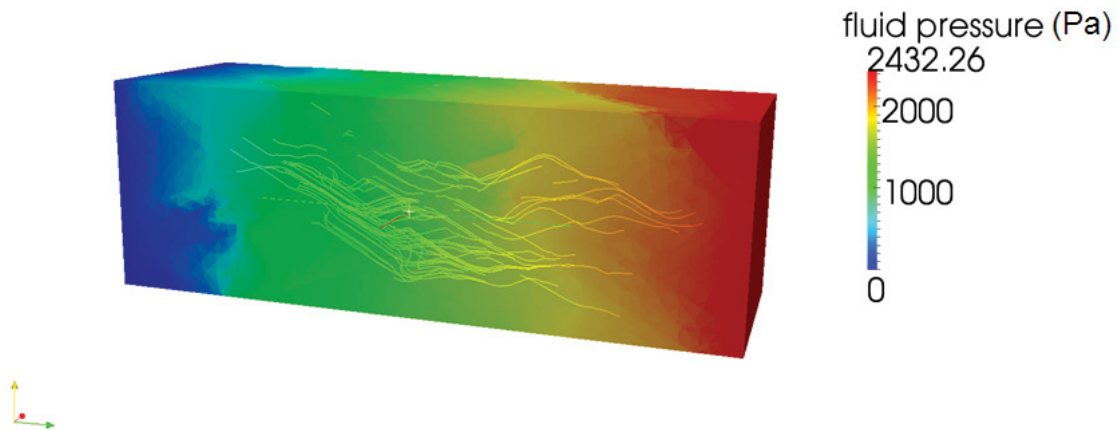
Figure 25: Streamline between two boundaries (Model 1, no wells)
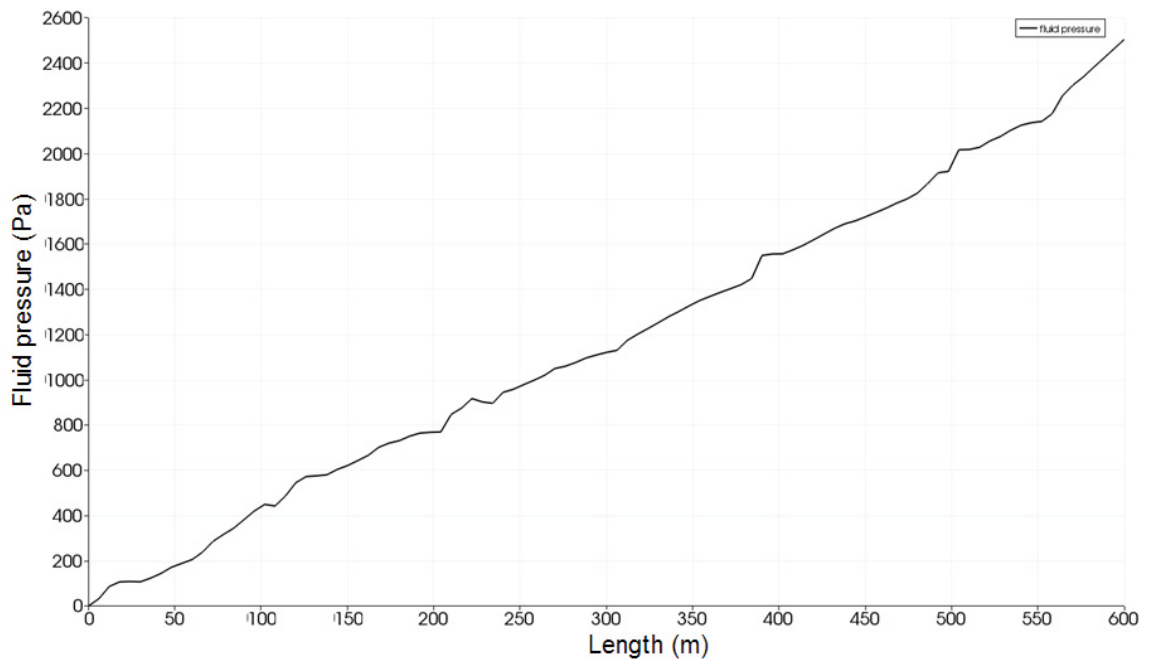
Figure 26: Pressure profile (Model 1, no wells)

In Figure 25, the path of fluid flow is irregular like streamline in other DFM models. Figure 26 shows that the pressure distribution in DFM model for linear flow is no longer straight compared to that in matrix-only models, because the pressure is influenced by fracture.

3.2 Comparison of k_{eff} for All DFM Models

In the last part of chapter 2, the pressures are calculated by analytical solution (Darcy's law with principle of superposition) and estimated by numerical methods (FEM analysis from CSMP++) with matrix-only model. During the comparison of results of both methods, the error between them is small (<5%). After verification of numerical methods, 8 DFM models, each is under three cases (radial flow, spherical flow and linear flow) are simulated by CSMP++. Table 8 and Table 9 indicate the result of effective permeability in each DFM models.

Table 8: The comparison of effective permeability for model 1-4

Name	Well Completion	Δp (Pa)	$P10$ (m^{-1})	k_{eff} (m^2)
Model1	Box-model (linear)	35406.1		2.45E-13
	Full (radial)	34327.6	0.11	6.71E-13
	Partial (sphere)	53489.6	0.20	2.71E-12
Model2	Box-model (linear)	3235.4		2.68E-12
	Full (radial)	3281.4	0.10	7.02E-12
	Partial (sphere)	13149.3	0.30	1.10E-11
Model3	Box-model (linear)	3273.4		2.65E-12
	Full (radial)	3023.7	0.11	7.62E-12
	Partial (sphere)	10784.5	0.30	1.34E-11
Model4	Box-model (linear)	4875.0		1.78E-12
	Full (radial)	8526.6	0.13	2.70E-12
	Partial (sphere)	25831.2	0.20	5.61E-12

Table 9: The comparison of effective permeability for model 5-8

Name	Well Completion	Δp (Pa)	$P10$ (m^{-1})	k_{eff} (m^2)
Model5	Box-model (linear)	5289.0		1.64E-12
	Full (radial)	5018.6	0.11	4.59E-12
	Partial (sphere)	15192.2	0.30	9.54E-12
Model6	Box-model (linear)	2481.2		3.50E-12
	Full (radial)	2199.7	0.10	1.05E-11
	Partial (sphere)	6812.3	0.20	2.13E-11
Model7	Box-model (linear)	2627.5		3.30E-12
	Full (radial)	2589.9	0.12	8.89E-12
	Partial (sphere)	11240.6	0.20	1.29E-11
Model8	Box-model (linear)	2527.0		3.44E-12
	Full (radial)	2701.7	0.12	8.53E-12
	Partial (sphere)	12863.0	0.20	1.13E-11

Although the fracture properties in each model are different, that result to diverse k_{eff} in the end, it is easy to find the relationship between three cases in each model.

The effective permeability has small value for linear flow (no wells), an intermediate value for radial flow and a large value for spherical flow.

In group 1 (model1-4), model1 comparing to other model has low fracture intensity, so that the effective permeability is lower than other model. Model 2-4 have same fracture trend, plunge and intensity. But the range of truncation is different. We can find that, with the large fracture size result a large effective permeability.

In group 2 (model5-8), all models have same fracture intensity, compared to group 1. The mean fracture size in each model mainly depends on value of X_{min} (minimum fracture size). With X_{min} and exponent increasing, mean fracture size in model will increase. However, the effective permeability in those models keeps almost constant. Therefore, the mean fracture size is not mostly factor to influence the effective permeability.

In part of DFM models setup, we discuss that in reality, it is possible that partial completion wells intersect no fracture (P10=0). Therefore, a comparison of well intersecting fractures and well intersecting no fractures is essential.

Table 10: Δp and K_{eff} in modified model 5b-8b

	$P10\ (m^{-1})$	Δp (Pa)	$K_{eff}\ (m^2)$
Model5b	0	1.32E+07	1.10E-14
Model6b	0	4.71E+06	3.08E-14
Model7b	0	9.72E+06	1.49E-14
Model8b	0	1.09E+07	1.33E-14

Table 10 shows the pressure difference and effective permeability between two partial penetrating wells for case that well intersect no fractures. Model 5b-8b is based on the original model 5-8, but removing the fractures. Table 11 and Table 13 indicate a directly comparison of pressure difference and effective permeability in two cases.

Table 11: Comparison of Δp between original model5-8 and modified model 5b-8b

	P10 (m⁻¹)	Δp (Pa)	P10 (m⁻¹)	Δp (Pa)
Model5	0.3	15192.2	0	1.32E+07
Model6	0.2	6812.3	0	4.71E+06
Model7	0.2	11240.6	0	9.72E+06
Model8	0.2	12863.0	0	1.09E+07

Table 12: Comparison of k_{eff} between original model5-8 and modified model 5b-8b

	P10 (m⁻¹)	k_{eff} (m²)	P10 (m⁻¹)	k_{eff} (m²)
Model5	0.3	9.54E-12	0	1.10E-14
Model6	0.2	2.13E-11	0	3.08E-14
Model7	0.2	1.29E-11	0	1.49E-14
Model8	0.2	1.13E-11	0	1.33E-14

From above tables, we find that the pressure difference is extremely high for new models. The matrix of permeability is set as 1.0E-14 for all modified models. Effective permeability of all modified models are only a little large than the matrix of permeability, which is far lower than the original model. We can conclude if the fractures don't touch the wells, the k_{eff} between wells will be very small. It is very important for model design. If we create the models, that the wells penetrate no fracture, the permeability is tiny influenced by fractures properties.
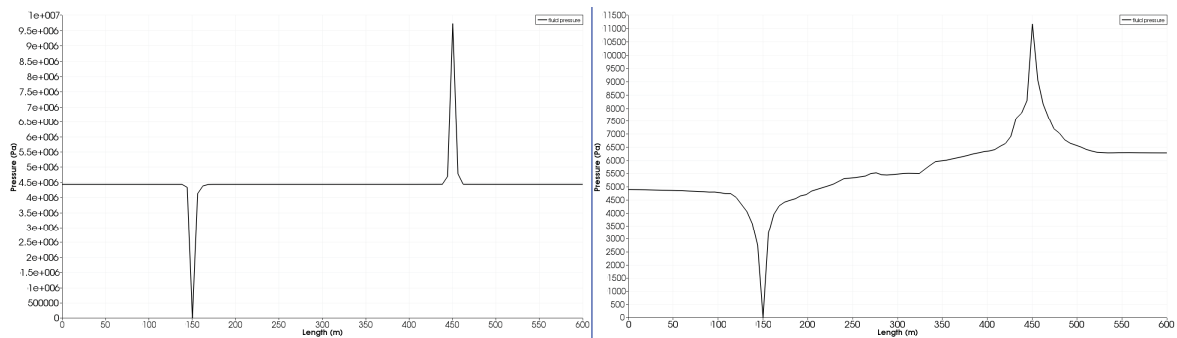
Figure 27: Comparison of pressure profile (left: modified model, right: original model)

To confirm our comparison, we select one pressure profile from all modified model and compare to original model (model 7). Pressure distribution of model 7b is similar to the matrix-only model, as if there's no fracture exists.

4. Discussion

The main purpose of this thesis is verification of numerical solution for simple steady-state, homogeneous models (Matrix-only), in order to apply the numerical solution to solve the complex, heterogeneous models (DFM). In this thesis, during the process of model establishment, the well will be designed as regular triangle instead of traditional circle. Comparing different radius approaches, it is found that the circumscribed triangle is quite corresponding to the circle. It obtains the smallest error for pressure estimation, comparing the numerical solution to analytical solution. If a regular triangle with same perimeter of circle well is used in numerical model, the error will be large instead. This is very important for well setup during establishment of model.

CSMP++ is based on FEM analysis. It is important to know that using smaller mesh size can refine the models, and cause a higher accurate simulation.

It is important to limit the maximum fracture size in the DFM models. If the maximum fracture size is above the distance between wells or boundaries, the single largest fracture will control the permeability of the region. The estimation of effective permeability in numerical solution will be with a low accuracy and purposeless.

Whether the wells intersect fractures will result an inverse result to effective permeability. If well intersect no fracture, the effective permeability between two wells is close to permeability of matrix, compared to the case that well penetrate fractures. Therefore, the contribution of fractures to the connectivity of models is very small, when wells intersect no fracture. It is significant for purpose of effective permeability estimation.

5. Conclusion

This thesis indicates the estimation of effective permeability by analytical solution (Darcy's law equation) and numerical solution (FEM analysis) for the homogeneous case (matrix-only model). Numerical solution is verified to analytical solution. After verification, effective permeability is estimated for complex DFM models through FEM analysis. Results from this thesis lead to following conclusion:

1. The effective permeability is calculated by derivative equation of Darcy's law, when the pressure is known from the steady-state FEM solution of the pressure equation as obtained with CSMP++. Results are analyzed applying analytical solutions to linear, spherical and radial flow. Where fractures are present so that no analytical solution can be obtained, a numerical reference solution is found by application of constant boundary pressure on opposite sides of the box-shaped model. The value of the effective permeability calculated this way is smaller than for the two other cases. The k_{eff} in spherical flow and radial flow therefore are overestimated.

2. The maximum element size of models in meshing software influences the accuracy of the results. A coarser model creates larger errors in result. Through comparison of mesh size 20m and 40m, a sensitivity analysis shows that an adaptive refinement placing many elements in regions with no-linear variations of pressure provides the best compromise between solution accuracy and computational effort.

3. The value of effective permeability is mainly related to fracture orientation, fracture size and fracture intensity. Through comparison of estimated k_{eff} for all DFM models, It is found that the effective permeability is increased with increasing fracture intensity (model1-2). Fracture orientation plays important role in influence to effective permeability. If the fractures link the wells directly, the effective permeability will be large (model 3-4). When the fracture intensity is used as input parameter, with the increasing mean fractures size, the k_{eff} is approximately constant (model 5-8). When wells penetrate no fractures, the effective permeability is small influenced by fractures properties.

References

Bourbiaux, B 2010, Oil & Gas Review, French Petroleum Institute IFP, Vol. 65, pp. 217-226.

Nelson, RA 2010, Geologic Analysis of naturally fractured reservoirs, 2nd edition, Gulf Professional Publishing, pp.43-48.

Masihi, M & King, PR 2006, Connectivity Prediction in Fractured Reservoirs With Variable Fracture, SPE 100229, SPE Annual Conference, Vienna

Durlofsky, J 1991, Numerical Calculation of Equivalent Grid Block Permeability Tensors for Heterogeneous Porous Media, Water Resources Research 27.

Nkashima, T & Sato,K 2000, Effective Permeability Estimation for Simulation of Naturally Fractured Reservoirs, SPE 64286, SPE Asia Pacific Oil and Gas Conference and Exhibition, Brisbane, Australia.

Matthews, CS & Russel, DG 1967, Pressure Buildup and Flow Tests in Wells, Society of Petroleum Engineers of AIME, pp.92-105.

Earlougher, RC 1977, Advances in Well Test Analysis, Society of Petroleum Engineers of AIME, pp.156-162.

Ahmed, U 1989, Permeability Estimation: The Various Sources and Their Interrelationships, SPE 19604, SPE Annual Technical Conference and Exihibition, Antonio.

Long, JCS & Gilmour, P 1985, A Model for Steady Fluid Flow in Random Three-Dimensional Networks of Disc-Shaped Fractures, Water Resources Research, Vol. 21, No. 8, University of California, Berkeley.

Snow, D 1969, Anisotropic Permeability of Fractured Media, Water Resources Research, Vol. 5, No.6, Colorado School of Mines, Colorado.

Warren, JE & Root, PJ 1963, The Behavior of Naturally Fractured Reservoirs, SPE Journal, Vol. 3, No. 3, pp.245-255.

Oda, M 1985, Permeability Tensor for Discontinuous Rock Masses, Geotechnique 35, No.4, pp.483-495.

Long, JC 1985, A Model for Steady Fluid Flow in Random Three-Dimensional Networks of Disc-Shaped Fractures, Water Resources Research, Vol. 21, No.8, pp.1105-1110

Robinson, PC 1984, Connectivity, Flow and Transport in Network Models of Fractured Media, St. Catherine's College, Oxford University.

Lough, MF 1996, A New Method to Calculate the Effective Permeability of Grid Blocks Used in the Simulation of Naturally Fractured Reservoirs, SPE 36730, SPE Annual Technical Conference and Exhibition,Denver.

Matthai, SK 2008, Numerical Simulation of Geomechanic Fracture Networks : application to Measuring Effective Permeability Variability, ARMA 08-295, 42nd US rock mechanis symposium and 2nd U.s.-Canada Rock Mechanics Symposium, San Francisco.

Tek, MR 1957, Development of a Generalized Darcy Equation, Journal of Petroleum Technology, Vol. 9, No. 6, pp.45-47.

Nordahl, K & Ringrose, P 2008, Identifying the Representative Elementary Volume for Permeability in Heterolithic Deposits Using Numerical Rock Models, Mathematical Geosciences Vol. 40, No. 7, pp. 753-771.

Bear, J 1972, Dynamics of Fluids in Porous Media, American Elsevier, New York.

Willhite, G 1986, Waterflooding, SPE Textbook Series Vol. 3, pp. 53-69.

Matthai, SK 2005, Control-Volume Finite-Element Two-Phase Flow Experiments with Fractured Rock Represented by Unstructured 3D Hybrid Meshes, SPE 93341, SPE reservoir simulation symposium, Houston.

Carlson, ES & Latham, GV 1993, Discrete Network Modeling for Tight Gas Fractured Reservoirs , SPE 26122-MS, SPE Technical Journals.

Doe, TW 1990, Simulation Of Dual-Porosity Flow In Discrete Fracture Networks, PETSOC Conference Paper, Annual Technical Meeting, pp. 90-120.

Chen, ZX 2007, Reservoir Simulation: Mathematical Techniques in oil recovery, University of Calgary, Alberta, Canada, pp. 34-52

Peaceman, DW 1977, Fundamentals of Numerical Reservoir Simulation, Developments in Petroleum Science 6, Elsevier Scientific Publishing Company, New York.

Barker, JA, 1988, A generalized radial flow model for hydraulic tests in fractured rock, Water Resources Research, Vol. 24, No. 10, pp. 1796-1804.

Boris, L 1986, Simulation and Characterization of Naturally Fractured Reservoirs, Textbook of Reservoir Characterization, Published by Academic Press, pp.132-157.

Dershowitz, WS 1992, Interpretation of fracture spacing and intensity, Conference Paper, American Rock Mechanics Association, Santa Fe.

Bonnet E, 2001, Scaling of Fracture System in Geological Media, Geophysics Review 39, pp. 347-383

Trenton, T 1996, Are fault growth and linage models consistent with power law distributionf of fault lengths, Journal of Structureal Geolgy Vol. 18, pp.281-293.

Rossen, WR, 2000, Connectivity and Permeability in Fracture Networks Obeying Power-Law Statistics, SPE 59720, Permian Basin Oil and Gas Recovery Conference Midland, Texas.

Schroeter, T 2007, Superposition Principle and Reciprocity for Pressure Transient Analysis of Data From Interfering Wells, SPE 110465, SPE Annual Technical Conference and Exhibition, Anaheim, Califonia,

Craft, BC & Hawkins, MF 1991, Applied Petroleum Reservoir Engineering, SPE TEXTBOOK, pp 213-226.

Culham, WE 1974, Pressure Buildup Equations for Spherical Flow Regime Problems, SPE Journal Paper, Vol. 14, No. 6, pp. 545-555.

Knott, JF 1976, Fundamentals of fracture mechanics, Butterworth & Co Publishers Ltd, London. pp.127-133.

Nomenclature

q= flow rate under steady condition (m^3/s)

A= cross section area for porous medium (m^2)

L = length of rock sample (m)

l_w: partial completion well length (m)

l_f: fracture length (m)

μ= fluid viscosity (Pa.s)

k= permeability of medium (m^2)

k_f= Fracture permeability

b= aperture size of fracture (m)

u= flow velocity (m/s)

Δp = pressure differential between two wells or two boundaries

p_i = initial pressure (psi)

p_r = average reservoir pressure (psi)

q_0 = current surface rate of flow (m^3/s)

r_w = radius of wellbore (m)

r_e = distance between wells and reservoir boundary (m)

h = reservoir thickness (m)

Φ = porosity, %

ρ = fluid density, kg/m^3

dp/dL= pressure gradient

k_{ij} = Permeability tensor

F_{ij} = Fracture tensor

F_{kk} = Total fractures

APPENDIX A

Monitor file for pressure estimation by CSMP++:

Groupname	Volume (m³)	Surface area (m²)
MATRIX	9.60E+06	880434
Model	9.60E+06	879246
WELL1	119.943	5.9999
WELL2	119.998	5.9999

Fluid pressure (Pa)

	MATRIX	Model	WELL1	WELL2
Minimum	100000	100000	224193	100000
Maximum	229189	229189	229189	100000

Calculation pressure difference and error in Maple:

> #*Wellbore radius*

> $r1 := evalf\left(\frac{1}{3} \cdot \left(\frac{\sqrt{3}}{2} \right) \right);$ # *Internally tangent circle*

  $r2 := evalf\left(\frac{2}{3} \cdot \left(\frac{\sqrt{3}}{2} \right) \right);$ # *Externally tangent circle*

$$r1 := 0.288676$$

$$r2 := 0.577349$$

> $r3 := 0.477 ;$

$$r3 := 0.477$$

>

#Pressure difference calculation for r1

po := 100000 ;   # Pa, pressure of production well

$q0 := \dfrac{1000}{86400}$;   # m3/s, production rate

$qi := -\dfrac{1000}{86400}$;   # m3/s, injection rate

$\mu := \dfrac{1}{1000}$;   # Pa·s, fluid viscosity

h := 200 ;   # m, reservoir thickness
k := 1e−12 ;   # m2, permeability
re := 300 ;   # m, wellbores distance

$$po := 100000$$

$$q0 := \frac{5}{432}$$

$$qi := -\frac{5}{432}$$

$$\mu := \frac{1}{1000}$$

$$h := 200$$

$$k := 1. \ 10^{-12}$$

$$re := 300$$

> $p := evalf\left(\dfrac{(q0 - qi)\cdot \mu}{\left(2\cdot(\pi)\cdot h\cdot k\right)} \cdot \ln\left(\dfrac{re}{r1}\right)\right)$;

$$p := 1.27955 \ \ 10^{5}$$

> $p1 := 129189$;

$$p1 := 129189$$

> $Err := evalf\left(\dfrac{p1 - p}{p1}\right)$

Errors by comparing the analytical solution to numerical solution, when using r1 as radius

$$Err := 0.00955190$$

>

> #Pressure calculation for r3

> $p := evalf\left(\dfrac{(q0 - qi)\cdot \mu}{\left(2\cdot(\pi)\cdot h\cdot k\right)} \cdot \ln\left(\dfrac{re}{r3}\right)\right)$;

$$p := 1.18704 \ \ 10^{5}$$

> $Err := evalf\left(\dfrac{p1 - p}{p1}\right)$
>
> # Errors by comparing the analytical solution to numerical solution, when using r3 as radius

$$Err := 0.0811602$$

APPENDIX B

Table 13: Fracture parameters for Model 1 (Group 1)

Fracture set	1	2
Fracture Intensity (P32)	0.02	0.02
Trend (degree)	150	120
Plunge (degree)	75	15
Min. Size of Truncate (m)	2	2
Max. Size of Truncate (m)	150	150
Total Fracture number	298	

Table 14: Fracture parameters for Model 2 (Group 1)

Fracture set	1	2
Fracture Intensity (P32)	0.04	0.035
Trend (degree)	30	160
Plunge (degree)	65	70
Min. Size of Truncate (m)	2	2
Max. Size of Truncate (m)	150	150
Total Fracture number	495	

Table 15: Fracture parameters for Model 3 (Group 1)

Fracture set	1	2
Fracture Intensity (P32)	0.035	0.04
Trend (degree)	30	160
Plunge (degree)	65	70
Min. Size of Truncate (m)	20	20
Max. Size of Truncate (m)	300	300
Total Fracture number	482	

Table 16: Fracture parameters for Model 4 (Group 1)

Fracture set	1	2
Fracture Intensity (P32)	0.035	0.04
Trend (degree)	30	160
Plunge (degree)	65	70
Min. Size of Truncate (m)	2	2
Max. Size of Truncate (m)	300	300
Total Fracture number	443	

Table 17: Fracture parameters for Model 5 (Group 2)

Fracture set	1	2
Fracture Intensity (P32)	0.04	0.04
Trend (degree)	150	120
Plunge (degree)	75	15
X_{min}	10	10
Exponent	1.5	1.5
Min. Size of Truncate (m)	2	2
Max. Size of Truncate (m)	200	200
Total Fracture number	500	

Table 18: Fracture parameters for Model 6 (Group 2)

Fracture set	1	2
Fracture Intensity (P32)	0.04	0.04
Trend (degree)	30	160
Plunge (degree)	65	70
X_{min}	20	20
Exponent	1.9	1.9
Min. Size of Truncate (m)	2	2
Max. Size of Truncate (m)	200	200
Total Fracture number	**397**	

Table 19: Fracture parameters for Model 7 (Group 2)

Fracture set	1	2
Fracture Intensity (P32)	0.04	0.04
Trend (degree)	30	160
Plunge (degree)	65	70
X_{min}	30	30
Exponent	2.8	2.8
Min. Size of Truncate (m)	2	2
Max. Size of Truncate (m)	200	200
Total Fracture number	**446**	

Table 20: Fracture parameters for Model 8 (Group 2)

Fracture set	1	2
Fracture Intensity (P32)	0.04	0.04
Trend (degree)	30	160
Plunge (degree)	65	70
X_{min}	40	40
Exponent	3.5	3.5
Min. Size of Truncate (m)	2	2
Max. Size of Truncate (m)	200	200
Total Fracture number	**323**	

APPENDIX C
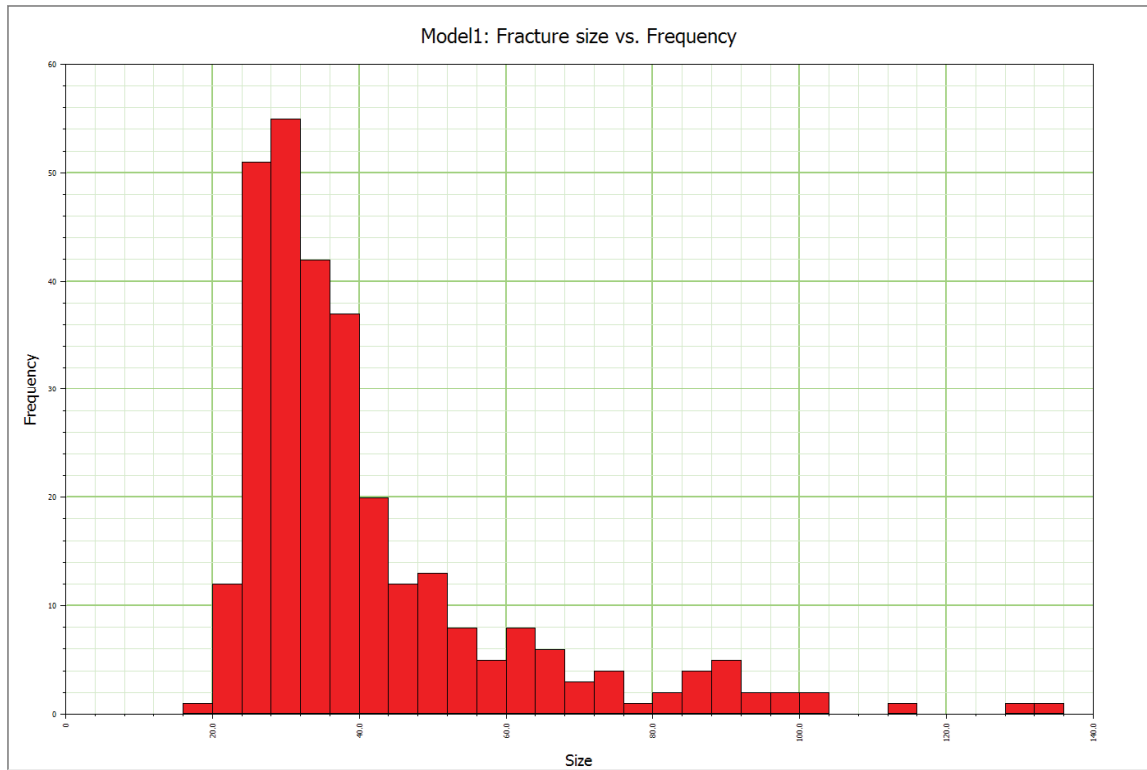
Figure 28: Model 1, Power law distribution, X_{min}= 26, Exponent= 2.85, Truncate= 2-150 m
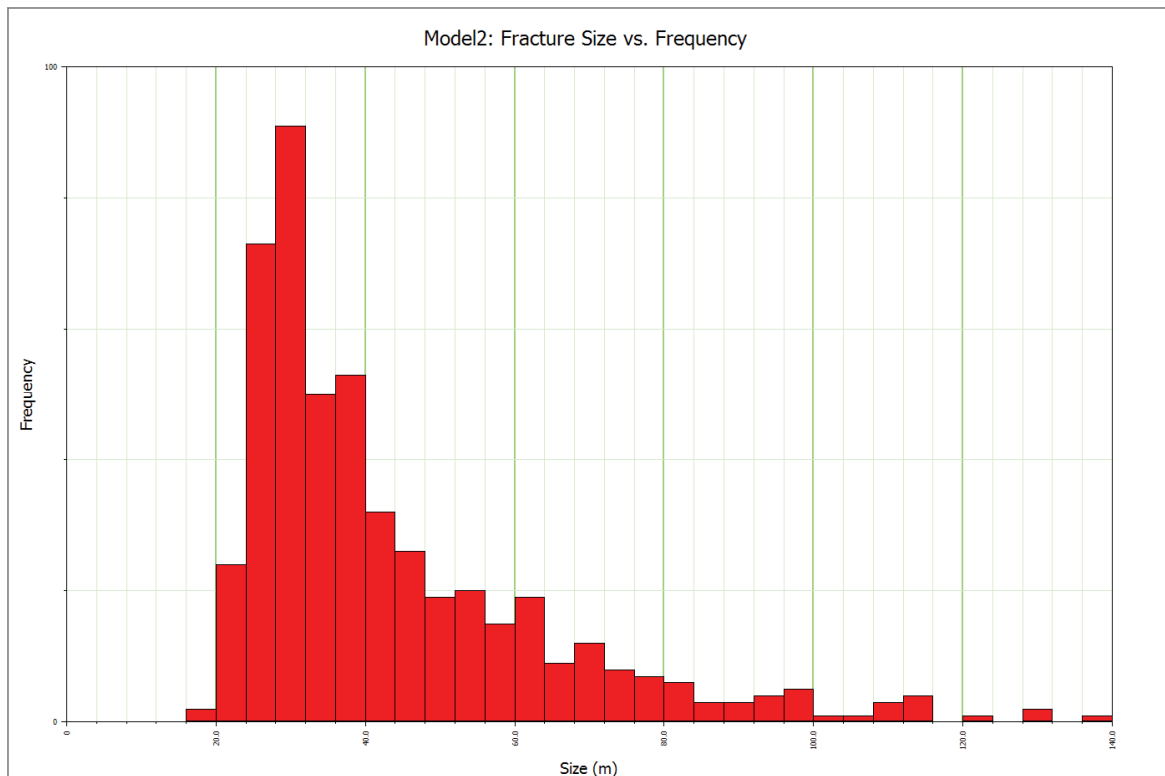
Figure 29: Model 2, Power law distribution, X_{min}= 26, Exponent= 2.85, Truncate= 2-150 m
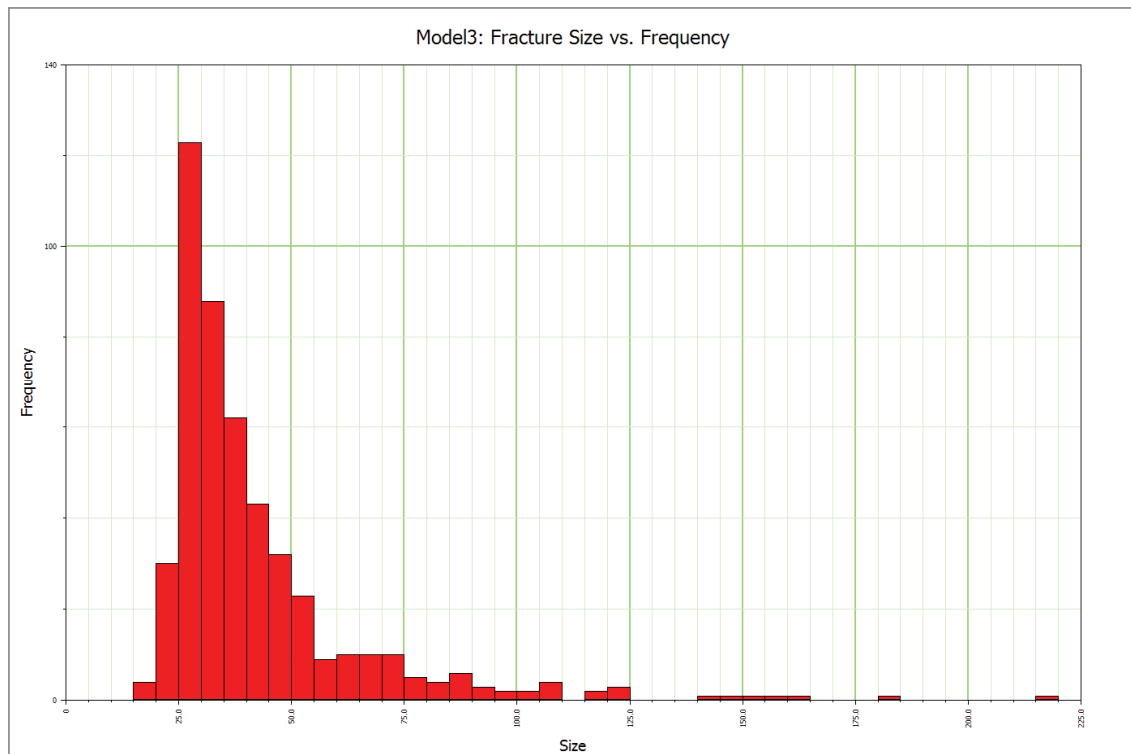
Figure 30: Model 3, Power law distribution, X_{min}= 26, Exponent= 2.85, Truncate= 20-300 m
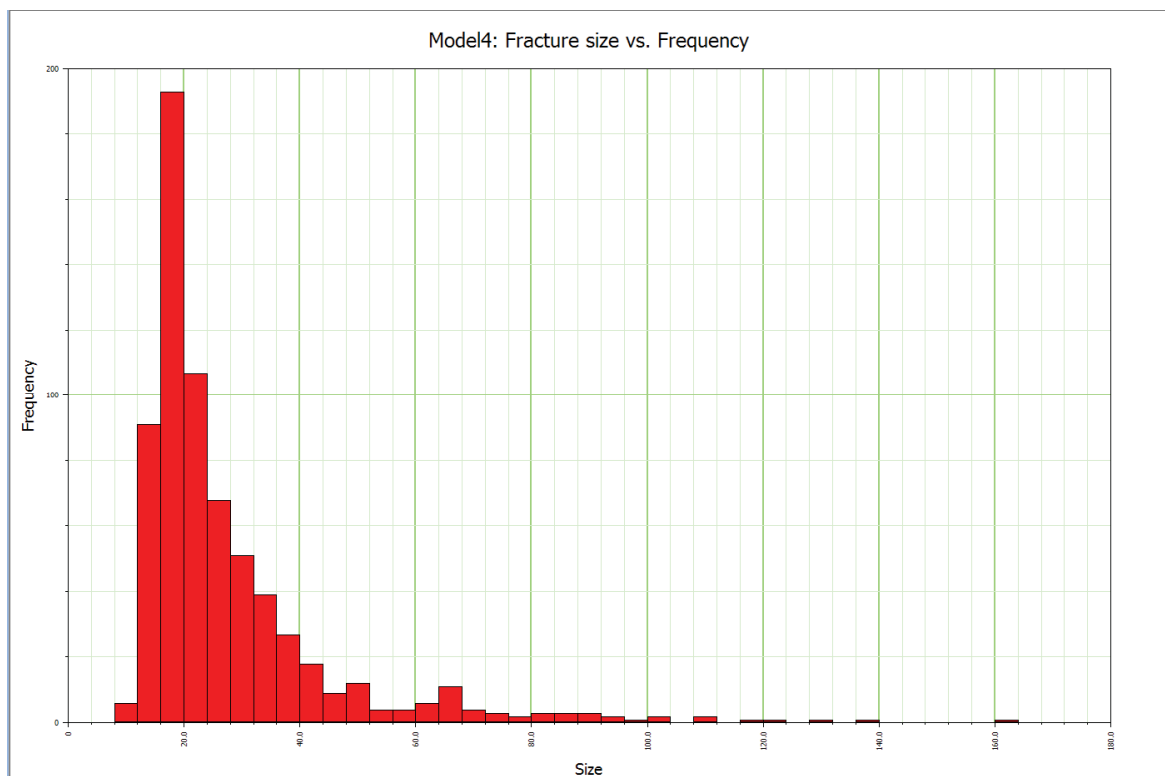
Figure 31: Model 4, Power law distribution, X_{min}= 26, Exponent= 2.85, Truncate= 2-300 m
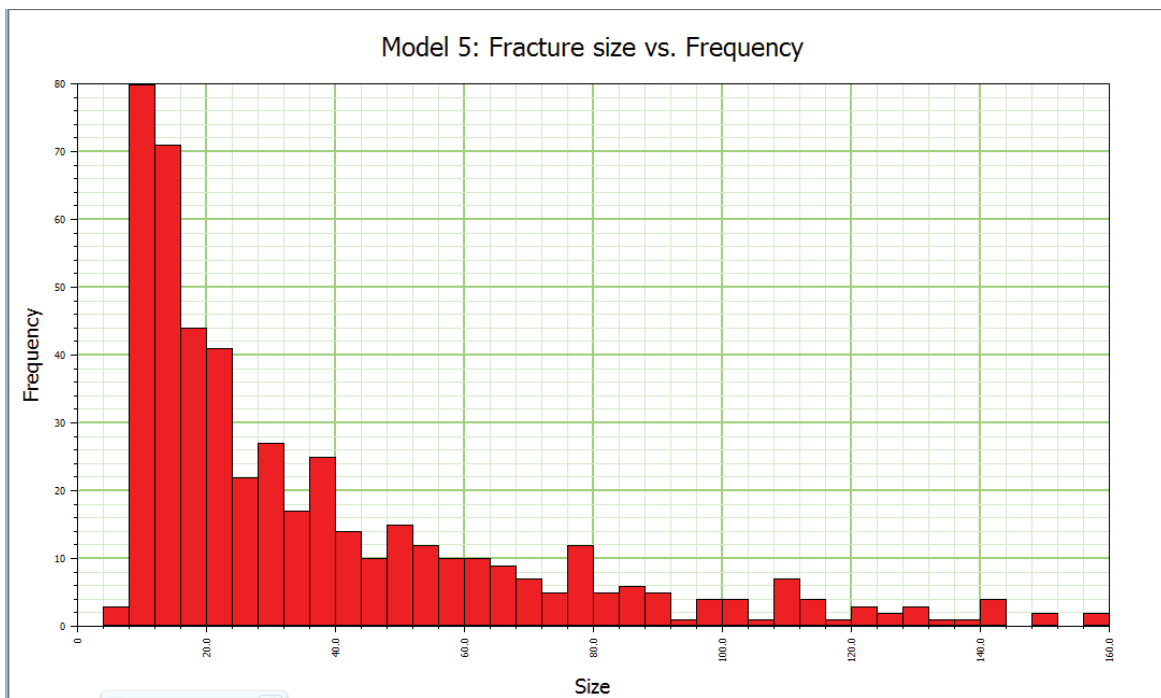
Figure 32: Model 5, Power law distribution, X_{min}= 10, Exponent= 1.6, Truncate: 2-200m
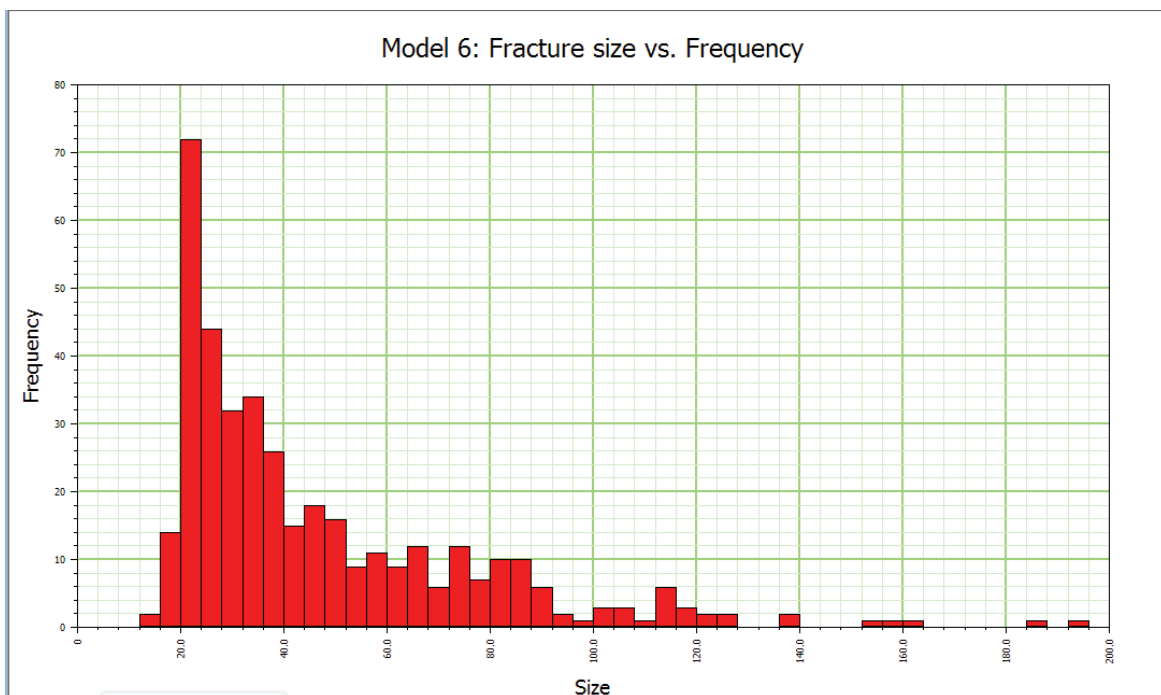
Figure 33: Model 6, Power law distribution, X_{min}= 20, Exponent= 1.9, Truncate: 2-200m
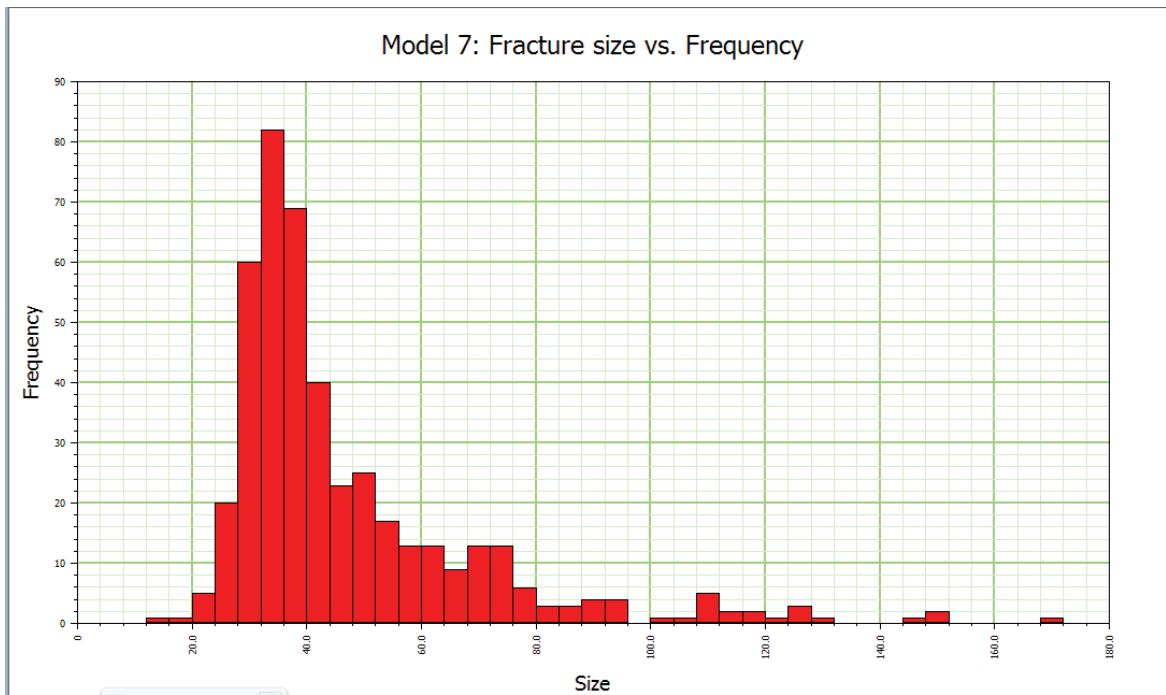
Figure 34: Model 7, Power law distribution, X_{min}= 30, Exponent= 2.8, Truncate: 2-200m
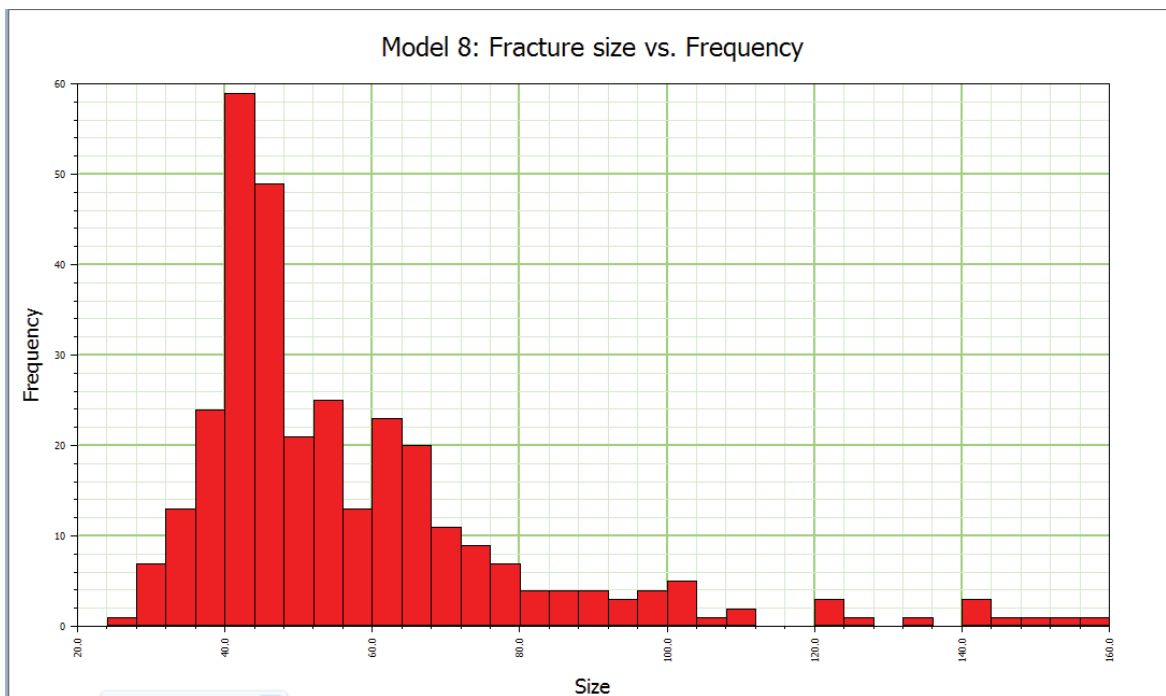
Figure 35: Model 8, Power law distribution, X_{min}= 40, exponent= 3.5, Truncate: 2-200m

APPENDIX D

An overview of fractures in fracture modeling software:
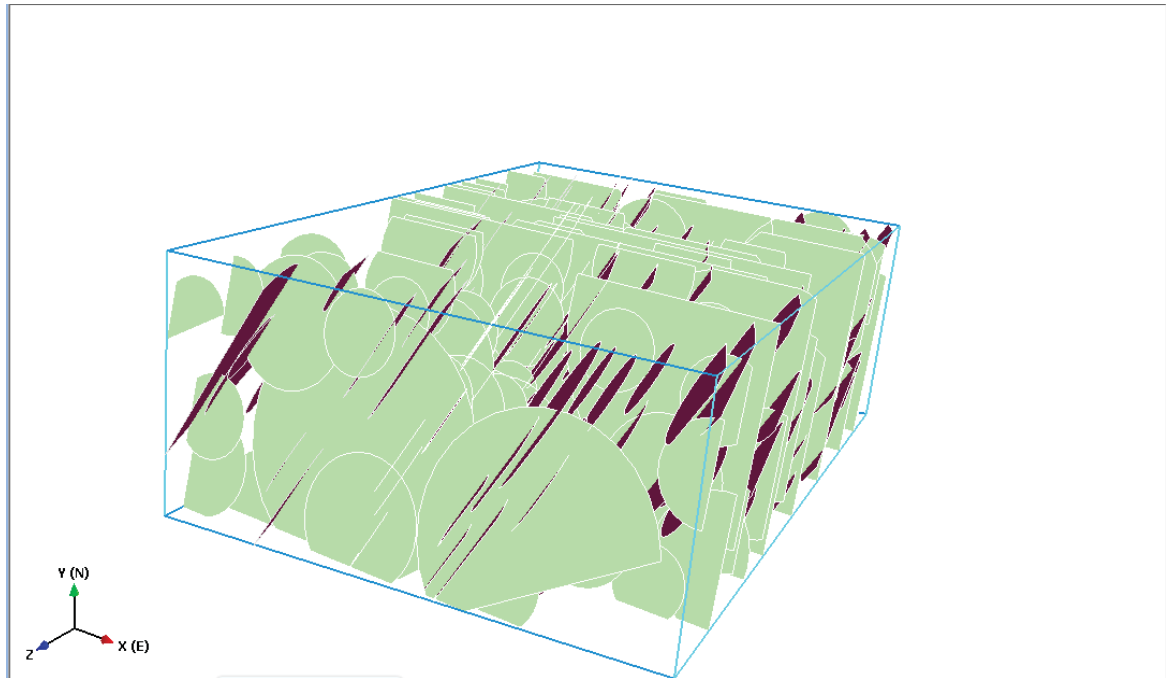
Figure 36: Fracture sets in FracMan (Model 1)
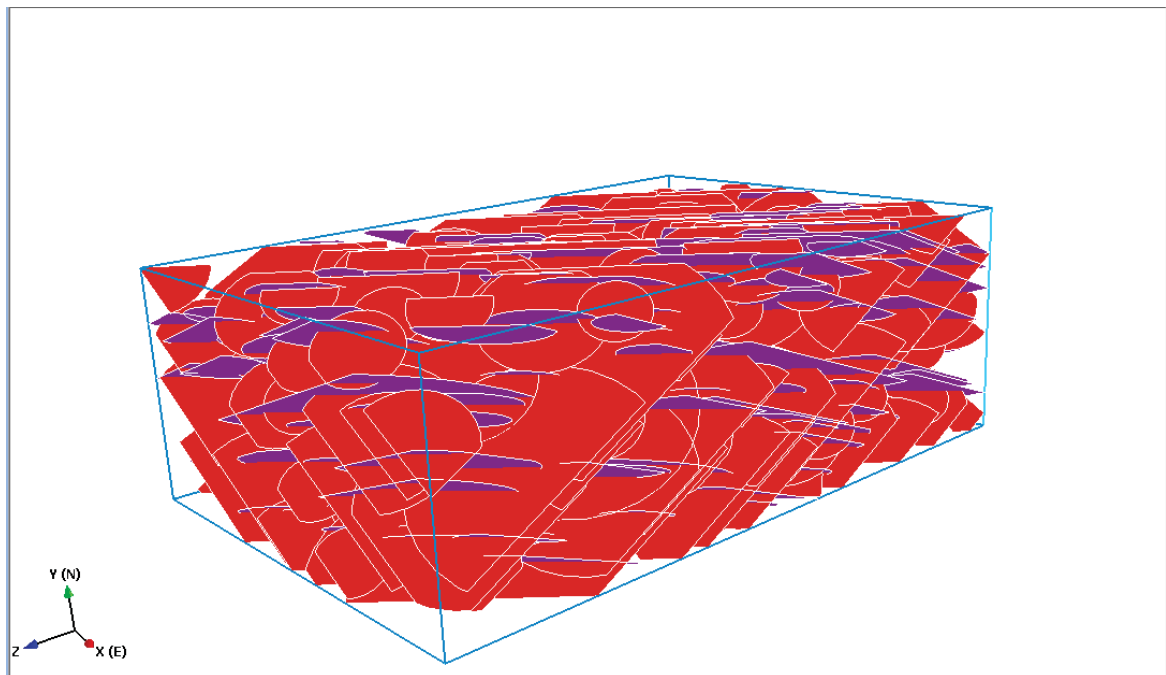
Figure 37: Fracture sets in FracMan (Model 2)
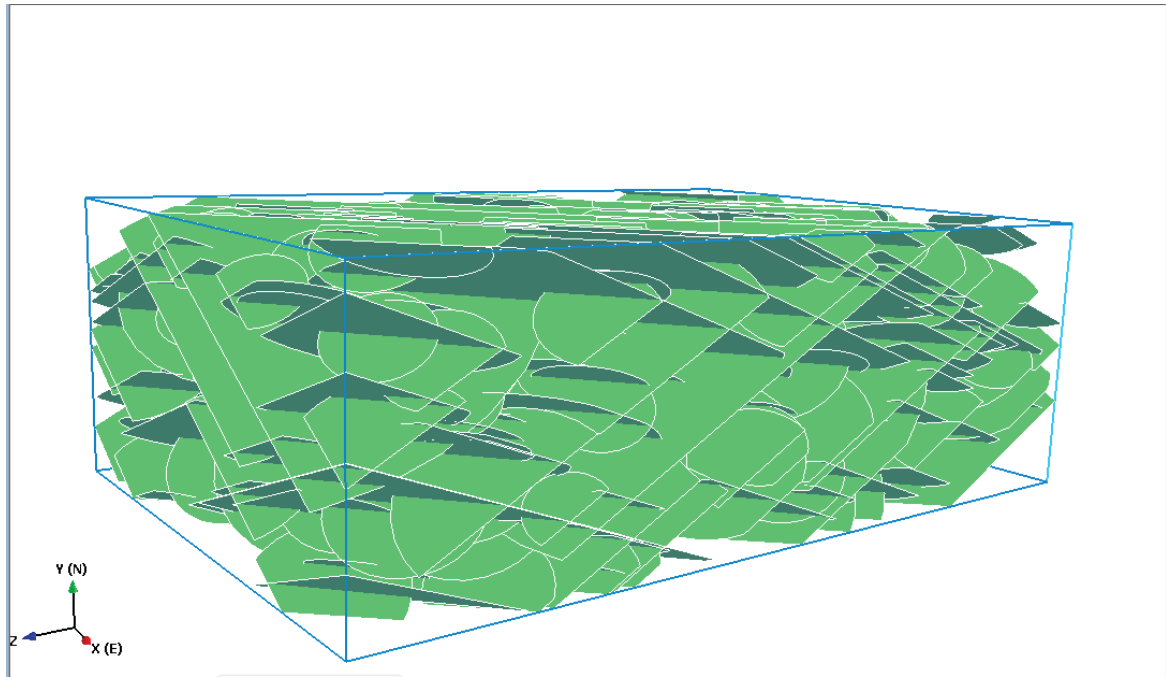
Figure 38: Fracture sets in FracMan (Model 3)
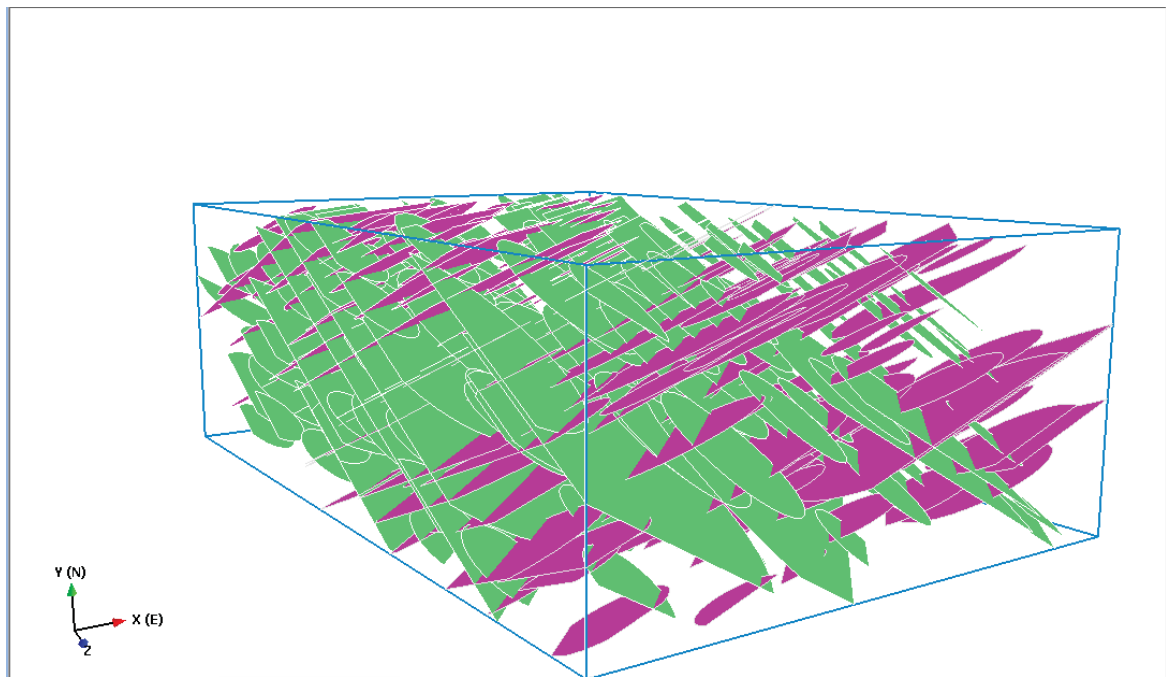
Figure 39: Fracture sets in FracMan (Model 4)
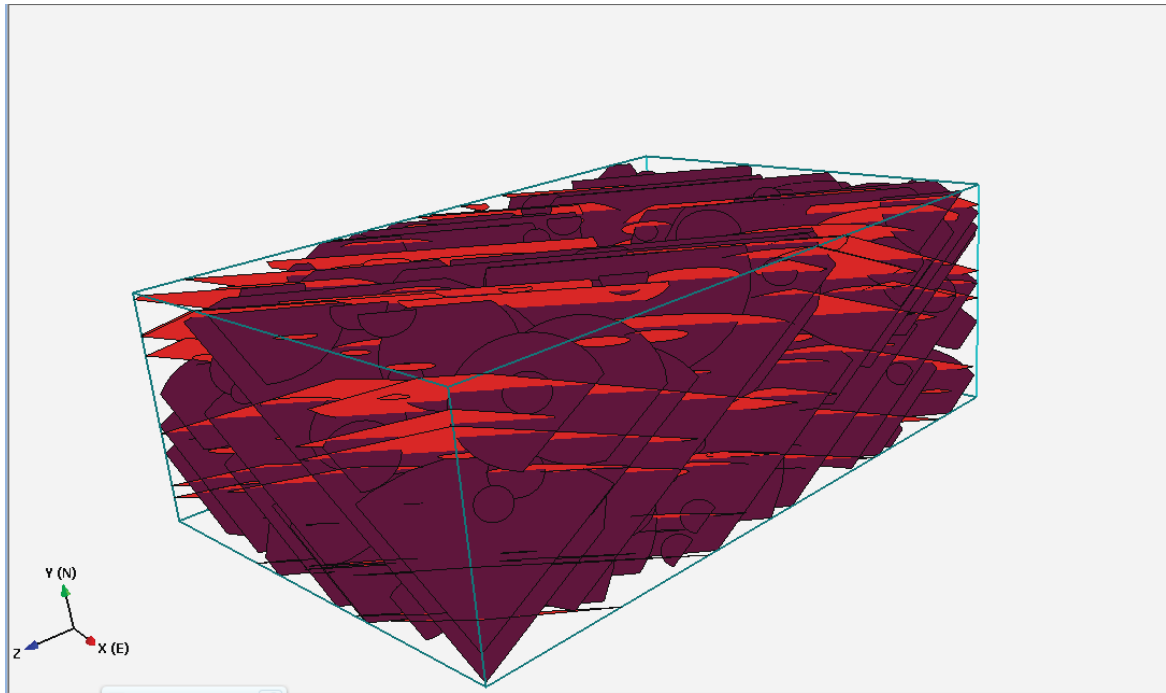
Figure 40: Fracture sets in FracMan (Model 5)
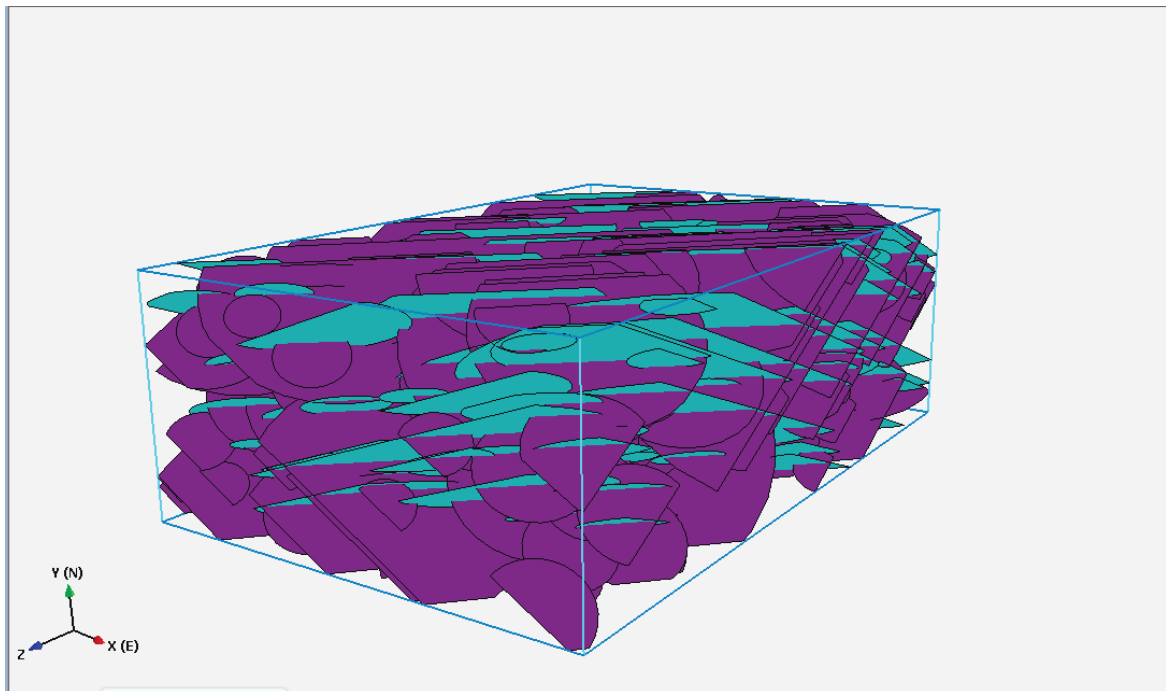
Figure 41: Fracture sets in FracMan (Model 6)
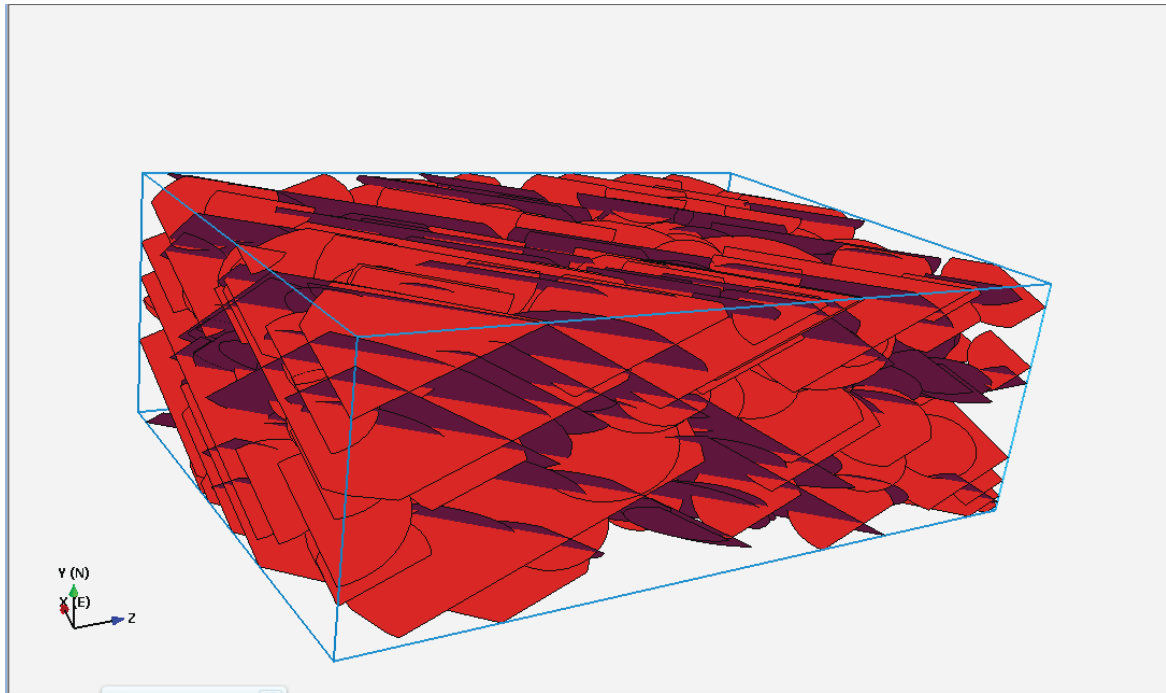
Figure 42: Fracture sets in FracMan (Model 7)
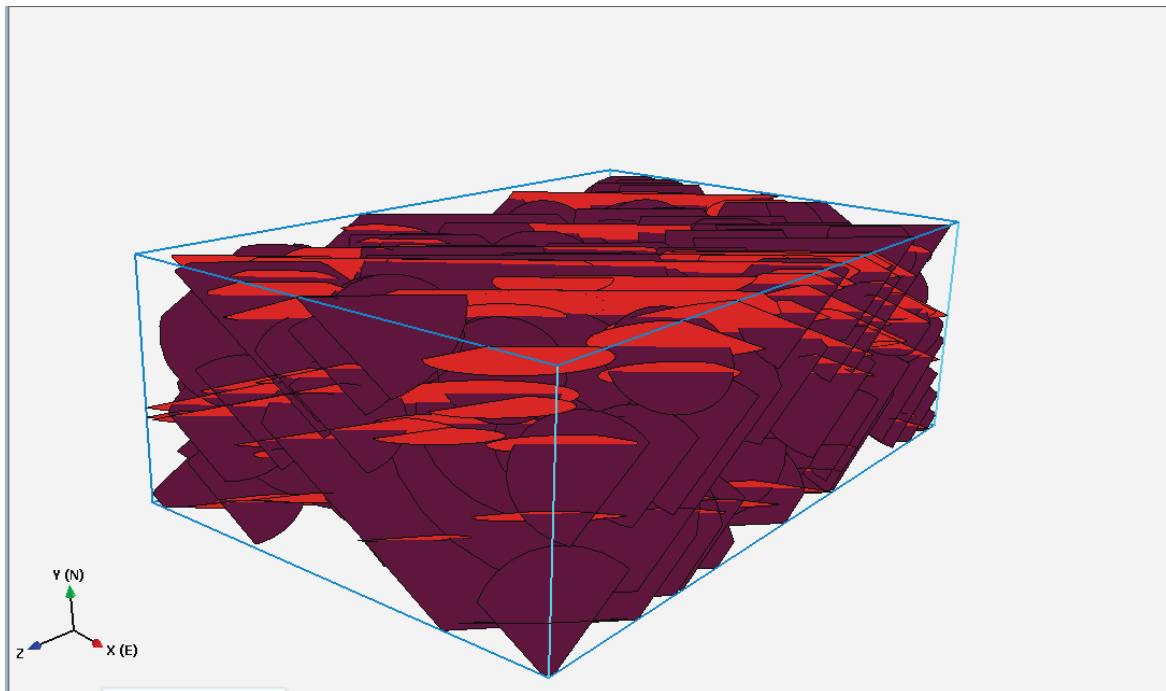
Figure 43: Fracture sets in FracMan (Model 8)

APPENDIX E

Mesh size=20 m

># *model parameters*

>
$$q := \frac{100}{86400};\qquad \# \ m3/s, \ flow \ rate$$

$$\mu := \frac{1}{1000};\qquad \# \ Pa \cdot s, \ fluid \ viscosity$$

$k := 1e - 14;\qquad \# \ m2, \ permeability \ of \ matrix$

$re := 300;\qquad \# \ m, \ two \ well \ distance$

$rw := 0.289;\qquad \# \ m, \ wellbore \ radius$

$lw := 5;\qquad \# \ m, \ partial \ well \ length$

$l := 600;\qquad \# \ m, \ two \ boundary \ distance$

$h := 200;\qquad \# \ m, \ full \ completion \ height$

$$q := \frac{1}{864}$$

$$\mu := \frac{1}{1000}$$

$$k := 1. \ 10^{-14}$$

$$re := 300$$

$$rw := 0.289$$

$$lw := 5$$

$$l := 600$$

$$h := 200$$

># *radial flow*

> $$p := evalf\left(\frac{2 \cdot q \cdot \mu}{\left(2 \cdot (\pi) \cdot h \cdot k \right)} \cdot \ln\left(\frac{\frac{re}{2}}{rw} \right) \right);$$

$$p := 1.15166 \ \ 10^{6}$$

> $p0 := 1231680;$
   $\#$ *pressure from CSMP* $++$

$$p0 := 1231680$$

> $$err1 := \frac{p0 - p}{p0};$$
   $\#$ *compareing the pressure in analytical solution with numerical solution*

$$err1 := 0.0469682$$

> # *sphericl flow*

> $p := evalf\left(\dfrac{4 \cdot q \cdot \mu}{4 \cdot (\pi) \cdot k} \cdot \left(\dfrac{1}{\frac{lw}{2}} - \dfrac{1}{\frac{re}{2}} \right) \right);$

$$p := 1.44910 \ 10^7$$

> $p0 := 13763600;$
    # *pressure from CSMP* ++

$$p0 := 13763600$$

> $err2 := \dfrac{p - p0}{p0};$
    # *compareing the pressure in analytical solution*
    with numerical solution

$$err1 := 0.0528495$$

> # *linear flow*

> $p := \dfrac{\frac{q}{200 \cdot 400} \cdot \mu \cdot l}{k};$

$$p := 8.68055 \ 10^5$$

> $p0 := 868018;$
    # *pressure from CSMP* ++

$$p0 := 868018$$

> $err3 := \dfrac{(p - p0)}{p};$
    # *compareing the pressure in analytical solution*
    with numerical solution

$$err3 := 0.0000426240$$

>